A Staggered Lattice Boltzmann Method for the Radiative Transfer Equation

R. Ruyssen, R. Cottereau, Pierre Boivin

Graphical Abstract

A Staggered Lattice Boltzmann Method for the Radiative Transfer Equation

R. Ruyssen, R. Cottereau, P. Boivin,

Highlights

A Staggered Lattice Boltzmann Method for the Radiative Transfer Equation

R. Ruyssen, R. Cottereau, P. Boivin,

- The Staggered Lattice Boltzmann Method approximates numerically the solutions of the Radiative Transfer Equation.
- Like the Lattice Boltzmann Method, it uses a regular grid in space and a quadrature in the propagation directions.
- Unlike the Lattice Boltzmann Method, it uses different discretizations in time to exactly stream energy along the different directions.
- A traversal algorithm allows to scatter energy between directions that have different time discretizations.

A Staggered Lattice Boltzmann Method for the Radiative Transfer Equation

R. Ruyssen[a,b], R. Cottereau[a,*], P. Boivin[b],

[a] *Aix-Marseille Univ., CNRS, Centrale Marseille, LMA UMR 7031, 4 impasse Nikola Tesla, 13013 Marseille, France*
[b] *Aix Marseille Univ., CNRS, Centrale Marseille, M2P2 UMR 7340, 38 Rue Frédéric Joliot Curie, 13013 Marseille, France*

Abstract

This paper introduces a method for the numerical approximation of solutions of the mono-kinetic Radiative Transfer Equation, adapting some of the features of the Lattice Boltzmann Method. The main difference between the Radiative Transfer Equation and the Boltzmann Equation used in the classical Lattice Boltzmann Method framework lies in the constrained norm of the velocity field appearing in the advection operator. This small difference leads to *off-grid* propagation if one uses a regular lattice, as classically done for efficiency reasons. To recover on-grid propagation, this paper introduces a specific time discretization along each propagation directions and an original traversal algorithm to allow for scattering between different directions at common times. The algorithm involves only linear time interpolations so as to preserve the local nature of the Lattice Boltzmann Method. The direction quadrature follows the principles of the Discrete Ordinate Method. The relevance of the approach is illustrated on different two-dimensional problems and the results are compared to previously published numerical test-cases.

Keywords: Radiative Transfer, Lattice Boltzmann Method, Staggered time discretizations.

1. Introduction

The Radiative Transfer Equation (RTE) is a complex integro-differential equation describing the evolution of the radiation intensity in absorbing, emitting and scattering media [1, 2]. It appears in many other areas of physics. For example in the kinetic theory of gases, under Boltzmann Equation (BE), it describes the statistical evolution of a system of moving and colliding particles (see e.g. [3] and the historical references therein). It also appears in the context of large-scale wave propagation modeling, where it describes the transport of energy density in the high frequency regime and when the environment has heterogeneous material parameters that fluctuate rapidly [4–6]. Its analytical solution is not generally possible, except in certain simple cases [7]. Therefore the use of numerical methods to obtain approximated solutions is necessary. Many different numerical methods have been developed to this end. They are generally categorized in literature into two groups (see e.g. [8]). The first group of methods is based on ray tracing, such as the zonal method [9, 10], the Ray Tracing Method [11, 12], the Discrete Transfer Method [13, 14] or the Monte Carlo Method (MCM) [15, 16]. However methods of MCM type are sometimes difficult to apply because of their slow convergence rate ($1/\sqrt{N}$ with N the number of sampled points), even

*regis.cottereau@cnrs.fr

if it is independent of the problem dimensionality. The second group of methods is based on discretizing partial differential equations. They usually combine several approaches to discretize the different problem dimensions such as the Finite Difference Method [17], the Finite Volume Method [18, 19], the Finite Element Method [20, 21], the Discrete Ordinate Method (DOM) [22–25], the Meshless Method [26], the Radial Basis Functions Method [27] or recently Reduced Order Models [28]. Nevertheless, because the problem dimensionality is large (seven dimensions in three-dimensional space), these approaches become expensive from computational time and memory consumption points of view. Recently, new methods have emerged, based on the Lattice Boltzmann Method (LBM).

The LBM has been historically developed in the field of fluid mechanics to solve the Navier-Stokes Equations (NSE). It has demonstrated a great efficiency for the simulation of compressible flows at low-Mach number and is still the object of numerous developments, notably for high speed flows (see e.g. [29, 30]). Its principle is to solve a problem based on a modified/simplified BE and whose solution macroscopically satisfies the NSE. This strategy has been generalized to other types of equations than the NSE, and the LBM can today be seen as a set of numerical methods to solve coupled conservation equations [31–34]. The different works using the LBM can be categorised into three groups.

A first set of approaches, which is historically the first one developed with the paper [35], adapts the LBM to solve the macroscopic steady diffusion equation which approximates the RTE in highly scattering regimes, see e.g. [36–39] and [40] for a rigorous established link between the adapted LBM and the macroscopic target diffusion equation.

A second set, initially developed by [41] for the steady RTE and later in [42] and [8] for the unsteady RTE, aims to solve the system of coupled convection equations arising from the discretization in direction of the RTE. To solve this equation system, the developments realized for the general case of convection-diffusion equations, as for example in the paper [43] (which extends those in [44]), are adapted and a LBM scheme is used for each system equation. The major drawback of this approach is that it becomes very heavy from a memory point of view.

Finally, the work of [45] recently proposed to adapt some of the LBM ingredients used to discretize the BE to the RTE. The main difference between the RTE and the BE lies in the constrained norm of the velocity field appearing in the advection operator. This small difference leads to *off-grid* propagation if one uses a regular lattice as done classically in the LBM. To overcome this difficulty, the authors propose to use a space interpolation scheme. However, a drawback of this approach is that space interpolation is numerically expensive and may introduce spatial diffusion.

In this work, we introduce a new numerical approach, called the Staggered Lattice Boltzmann Method (SLBM), which in the vein of [45] adapts also some of the LBM features to the RTE, but with the advantage to recover the *on-grid* property of LBM.

Our paper is structured as follows. In the following section 2, we summarize the classical LBM features when used to solve the NSE. In the section 3, after recalling the continuous RTE and the main differences it has with BE, we briefly detail the main existing strategies, based on LBM, for its numerical solution and we finish by introducing the principle of the SLBM approach we propose and the advantages it brings. We then present, in the section 4, its different ingredients: the construction of special discrete sets of directions with associated time lattices and quadratures, the introduction of a new fully discrete formulation of the RTE and the use of a particular solution algorithm. In section 5 the relevance of our approach is enlightened by two-dimensional tests and the solution we obtain are compared with others taken from literature. Conclusions are given in section 6.

2. Brief summary of the Lattice Boltzmann Method for Navier-Stokes Equations solution

In this section we briefly introduce the LBM features for the Navier-Stokes Equations solution.

2.1. The macroscopic model

We consider a flowing fluid $\mathcal{F}$ passing through the closure of a bounded and sufficiently regular open domain $\Omega \subset \mathbb{R}^d$ (with $d = 1, 2$ or 3), which boundary is denoted $\partial\Omega$, over a time interval $I =]0, T]$ (with $T \in \mathbb{R}_+^\star$). We equip $\mathbb{R}^d$ with an Euclidian orthonormal frame $(\mathbf{O},\ \mathbf{e}_1, \ldots,\ \mathbf{e}_d)$. The fluid motion is described, at macroscopic scale, by the Navier-Stokes Equations (NSE) which form a system of partial differential equations formulated in terms of its velocity $\mathbf{u}$, pressure p and density ρ fields. All these fields are functions of time t and position $\mathbf{x}$ in the time-space domain $I \times \Omega$. These equations read, $\forall\, (t, \mathbf{x}) \in I \times \Omega$:

$$\frac{\partial \rho}{\partial t}(t, \mathbf{x}) + \nabla \cdot (\rho \mathbf{u})\,(t, \mathbf{x}) = 0 \qquad \text{(Mass conservation)} \tag{1}$$

$$\frac{\partial \rho \mathbf{u}}{\partial t}(t, \mathbf{x}) + \nabla \cdot (\rho \mathbf{u} \otimes \mathbf{u} - \boldsymbol{\sigma}\,(p, \mathbf{u}))\,(t, \mathbf{x}) = \rho \mathbf{f}(t, \mathbf{x}) \qquad \text{(Momentum conservation)} \tag{2}$$

where, $\otimes$ is the tensor product, $\mathbf{f}$ is a density of body forces to which the fluid is submitted and where we have assumed that the flow is isothermal:

$$p = \rho c_s^2, \tag{3}$$

where c_s is the sound speed. We further assume that the fluid is Newtonian, homogeneous and weakly compressible, such that, its constitutive relation, relating its stress tensor field $\boldsymbol{\sigma}$ to its pressure and strain tensor field $\boldsymbol{\epsilon}$, reads (see e.g. [46]):

$$\boldsymbol{\sigma}\,(p, \mathbf{u}) = 2\mu \boldsymbol{\epsilon}\,(\mathbf{u}) - \left(\frac{2}{3}\mu \mathrm{Tr}\,(\boldsymbol{\epsilon}\,(\mathbf{u})) + p\right) \boldsymbol{I} \tag{4}$$

where μ is the fluid shear viscosity, $\boldsymbol{I}$ the identity tensor and where we have neglected the bulk viscosity. The strain tensor field is defined as:

$$\boldsymbol{\epsilon}\,(\mathbf{u}) = \frac{1}{2}\left(\boldsymbol{\nabla}\mathbf{u} + (\boldsymbol{\nabla}\mathbf{u})^T\right). \tag{5}$$

We add to equations (1)-(5), initial conditions, that read:

$$\rho(0, \mathbf{x}) = \rho_0(\mathbf{x}),\ \text{and}\ \mathbf{u}(0, \mathbf{x}) = \mathbf{u}_0(\mathbf{x}),\ \forall \mathbf{x} \in \Omega, \tag{6}$$

where ρ_0 and $\mathbf{u}_0$ are given fields, as well as Dirichlet boundary conditions:

$$\rho(t, \mathbf{x}) = \rho_d(t, \mathbf{x}),\ \text{and}\ \rho\mathbf{u}(t, \mathbf{x}) = \rho\mathbf{u}_d(t, \mathbf{x}),\ \forall\, (t, \mathbf{x}) \in I \times \Gamma_D, \tag{7}$$

and Neumann boundary conditions:

$$\rho\mathbf{u}(t, \mathbf{x}) \cdot \mathbf{n} = \phi^\rho(t, \mathbf{x})\ \text{and}\ (\rho\mathbf{u} \otimes \mathbf{u} - \boldsymbol{\sigma}\,(p, \mathbf{u}))\,\mathbf{n} = \boldsymbol{\phi}^{\rho\mathbf{u}}(t, \mathbf{x}),\ \forall\, (t, \mathbf{x}) \in I \times \Gamma_N, \tag{8}$$

where Γ_D and Γ_N form a partition of $\partial\Omega$ without overlapping ($\Gamma_D \cup \Gamma_N = \partial\Omega$ and $\Gamma_D \cap \Gamma_N = \varnothing$) and ρ_d, $\rho\mathbf{u}_d$, ϕ^ρ, $\boldsymbol{\phi}^{\rho\mathbf{u}}$ are given fields.

2.2. The simplified Mesoscopic model

In kinetic theory, the motion of a fluid is described, at mesoscopic scale, by the BE. It is an integro-differential equation formulated in terms of a distribution function a. It is a function of $(t, \mathbf{x})$ but also of velocity $\mathbf{v}$ in the phase domain $I \times \Omega \times \mathbb{R}^d$. It gives the density of particles which, at t and located at $\mathbf{x}$, have a velocity $\mathbf{v}$. The BE reads, $\forall\, (t, \mathbf{x}, \mathbf{v}) \in I \times \Omega \times \mathbb{R}^d$:

$$\frac{\partial a}{\partial t}(t, \mathbf{x}, \mathbf{v}) + \mathbf{v} \cdot \nabla_{\mathbf{x}} a(t, \mathbf{x}, \mathbf{v}) = K[a](t, \mathbf{x}, \mathbf{v}) \tag{9}$$

where $K[a]$ is the integral collision operator modeling the particle collisions. In the context of the LBM, this integral collision operator is classically approximated by a local one, the simplest and best known being the Bhatnagar-Gross-Krook [47]:

$$K[a] \approx K_{\mathrm{BGK}}[a] = -\frac{1}{\tau}\left(a - a^{\mathrm{eq}}\right), \tag{10}$$

where $\tau > 0$ is the relaxation parameter related to the viscosity of the fluid (see e.g. the books [48, 49] for discussions on the link between τ and the LBM precision and stability). The equilibrium state is described by a^{eq} the equilibrium distribution function which, for classical fluid, is equal to the Maxwell-Boltzmann distribution [50]:

$$a^{\mathrm{eq}}(t, \mathbf{x}, \mathbf{v}) = \frac{\rho(t, \mathbf{x})}{(2\pi c_s^2)^{\frac{d}{2}}} \exp\left(-\frac{\|\mathbf{v} - \mathbf{u}(t, \mathbf{x})\|^2}{2c_s^2}\right). \tag{11}$$

The fluid density ρ and velocity $\mathbf{u}$ can be computed as the zeroth and first moment of the distribution function, respectively:

$$\rho(t, \mathbf{x}) = \int_{\mathbb{R}^d} a(t, \mathbf{x}, \mathbf{v}')\, \mathrm{d}\mathbf{v}' \text{ and } \rho\mathbf{u}(t, \mathbf{x}) = \int_{\mathbb{R}^d} \mathbf{v}' a(t, \mathbf{x}, \mathbf{v}')\, \mathrm{d}\mathbf{v}'. \tag{12}$$

Other collision operators with more degrees of freedom exist as the Two-Relaxation-Time (TRT) or the Multiple-Relaxation-Time (MRT) (see [49] and the references therein). Substituting the BGK collision operator from equation (10) into the equation (9) gives the BGK BE, the central element of LBM.

2.3. Speed discretization of the BGK Boltzmann Equation

An important feature of the LBM, giving it some of its effectiveness, is the idea to construct an approximation of the distribution function, following the steps of a collocation method, with respect to its dependence with $\mathbf{v}$. Starting from the equilibrium distribution function a^{eq}, the method consists in projecting a^{eq} onto the Hermite polynomials basis. In d dimensions, this projection takes the following form:

$$a^{\mathrm{eq}}(t, \mathbf{x}, \mathbf{v}) = \omega(\mathbf{v}) \sum_{k=0}^{\infty} \frac{1}{k!} \mathbf{a}^{\mathrm{eq},(k)}(t, \mathbf{x}) : \mathbf{H}^{(k)}(\mathbf{v}) \tag{13}$$

where : is the k-contraction product, $\mathbf{a}^{\mathrm{eq},(k)}(t, \mathbf{x})$ is defined as:

$$\mathbf{a}^{\mathrm{eq},(k)}(t, \mathbf{x}) = \int_{\mathbb{R}^d} a^{\mathrm{eq}}(t, \mathbf{x}, \mathbf{v}') \mathbf{H}^{(k)}(\mathbf{v}')\, \mathrm{d}\mathbf{v}' \tag{14}$$

with $\mathbf{H}^k$ the Hermite polynomials and ω the weighting function. These are defined as:

$$\mathbf{H}^{(k)}(\mathbf{v}) = \frac{(-1)^k}{\omega(\mathbf{v})} \nabla^k \omega(\mathbf{v}) \text{ and } \omega(\mathbf{v}) = \frac{1}{(2\pi)^{\frac{d}{2}}} \exp\left(-\frac{\|\mathbf{v}\|^2}{2}\right) \tag{15}$$

where ∇^k is a tensor of order k defined as:

$$\nabla^k \omega(\mathbf{v}) = \sum_{|\boldsymbol{\alpha}|=k} \frac{\partial^{|\boldsymbol{\alpha}|}\omega}{\partial v_1^{\alpha_1} \cdots \partial v_d^{\alpha_d}}(\mathbf{v}) \mathbf{e}_1^{\otimes \alpha_1} \otimes \cdots \otimes \mathbf{e}_d^{\otimes \alpha_d}, \quad \forall k \in \mathbb{N}, \tag{16}$$

with $\boldsymbol{\alpha} \in \mathbb{N}^d$, $|\boldsymbol{\alpha}| = \alpha_1 + \cdots + \alpha_d$ and $\mathbf{e}_i^{\otimes \alpha_i}$ the α_i tensor product of $\mathbf{e}_i$, i.e.:

$$\mathbf{e}_i^{\otimes \alpha_i} = \underbrace{\mathbf{e}_i \otimes \cdots \otimes \mathbf{e}_i}_{\alpha_i} \text{ where by convention we choose that } \mathbf{e}_i^{\otimes 0} = 1. \tag{17}$$

In fact, the first expansion coefficients $\mathbf{a}^{\mathrm{eq},(k)}$ are directly connected to the first moments of a^{eq} (see [49] for details), for example: $\mathbf{a}^{\mathrm{eq},(0)} = \rho$ and $\mathbf{a}^{\mathrm{eq},(1)} = \rho\mathbf{u}$. Thus, truncating the expansion given by equation (14) at a low order: N, provides a cheap and compact approximation of a^{eq} while conserving its first moments - the only ones included in the NSE. Also, since the collision operators classically used (e.g as the BGK operator given in equation (10)) conserve the first moments (mass and momentum – collisions are assumed to be elastic), the distribution function a can be approximated by the same Hermite decomposition, while preserving the macroscopic behavior. Moreover, because the distribution functions are decomposed on the Hermite basis, their moments can be exactly computed by the use of the Gauss-Hermite quadrature rule:

$$\int_{\mathbb{R}^d} \omega(\mathbf{v}') P^{(N)}(\mathbf{v}') \, \mathrm{d}\mathbf{v}' = \sum_{i=0}^{q-1} w_i P^{(N)}(\mathbf{v}_i) \tag{18}$$

where the $\mathbf{v}_i$ are the q roots of the Hermite polynomials, w_i the associated weight and $P^{(N)}$ a polynomial function of degree N defined on $\mathbb{R}^d$ (for the quadrature to be exact we must have $N \leqslant 2q-1$). The usual velocity and weight sets, used for the Gauss-Hermite quadrature rule, are generally denoted DdQq, with q the number of discrete velocities (see [49]). See for example the D2Q9 and D2Q13 speed sets represented in Figure 4 and whose associated weights are given by:

$$w_0 = \frac{4}{9}, \; w_i = \frac{1}{9} \; i \in [\![1,4]\!] \text{ and } w_i = \frac{1}{36} \; i \in [\![5,8]\!], \tag{19}$$

for the the D2Q9 set and:

$$w_0 = \frac{3}{8}, \; w_i = \frac{1}{12} \; i \in [\![1,4]\!], \; w_i = \frac{1}{36} \; i \in [\![5,8]\!] \text{ and } w_i = \frac{1}{96} \; i \in [\![9,12]\!], \tag{20}$$

for the the D2Q13 one. Afterwards, the BGK BE is imposed at the collocation points which are taken as the $\mathbf{v}_i$ and we define:

$$a_i^{\mathrm{eq}}(t,\mathbf{x}) = \frac{w_i}{\omega(\mathbf{v}_i)} a^{\mathrm{eq}}(t,\mathbf{x},\mathbf{v}_i) \text{ and } a_i(t,\mathbf{x}) = \frac{w_i}{\omega(\mathbf{v}_i)} a(t,\mathbf{x},\mathbf{v}_i). \tag{21}$$

If the discrete velocity set is well chosen, the distribution functions moments can be computed exactly as follows:

$$\rho(t,\mathbf{x}) = \sum_{i=0}^{q-1} a_i(t,\mathbf{x}) \quad \text{and} \quad \rho\mathbf{u}(t,\mathbf{x}) = \sum_{i=0}^{q-1} \mathbf{v}_i a_i(t,\mathbf{x}), \tag{22}$$

2.4. Link between the mesoscopic model and the macroscopic one

The interest in LBM comes from the link that can be made between the numerically solved mesoscopic modified/simplified model and the resulting macroscopic equations simulated. The most widely used method to establish this link is the Chapman-Enskog expansion. It is used in [49, Chapter 4] to show that a mesoscopic model with an equilibrium distribution function approximation truncated at the order $N = 2$, allows to verify the macroscopic model presented in subsection 2.1. The approximation reads:

$$a^{\mathrm{eq}}(t,\mathbf{x},\mathbf{v}) \approx \omega(\mathbf{v})\rho(t,\mathbf{x})\left[1 + \frac{\mathbf{v}\cdot\mathbf{u}(t,\mathbf{x})}{c_s^2} + \frac{(\mathbf{u}(t,\mathbf{x})\otimes\mathbf{u}(t,\mathbf{x})) : (\mathbf{v}\otimes\mathbf{v} - c_s^2\boldsymbol{I})}{2c_s^4}\right] \tag{23}$$

Other approaches than the Chapman-Enskog one exist, see for example [31, 34, 49] and the reference therein.
To extend the use of the LBM to other macroscopic models, it is possible to define general equilibrium distribution functions under a form closed to equation (23), unrelated to a Maxwell-Boltzmann distribution. Thus the LBM can be seen as a numerical solver losing its link with to kinetic theory of gases [31–34].

2.5. Fully discretized Boltzmann Equation

Classically, $\mathbb{R}^d$ is discretized in a d-dimensional lattice denoted $\mathcal{L}_{\mathbf{x}} = \Delta x \times \mathbb{Z}^d$ of constant step $\Delta x > 0$ in the d directions (we implicitly impose that the basis vectors of $\mathbb{R}^d$ frame we have introduced, i.e. $\mathbf{e}_1, \ldots, \mathbf{e}_d$, are the principal axes of $\mathcal{L}_{\mathbf{x}}$) and the time interval I is discretized in a 1-dimensional lattice $\mathcal{L}_t = \Delta t \times [\![0, N_t]\!]$ of constant step $\Delta t > 0$. To pose the discrete problem the nodes of $\mathcal{L}_{\mathbf{x}}$ are separated into several groups, see Figure 2:

- the internal nodes: $\mathcal{I}_{\mathrm{in}} = \{\mathbf{x} \in \mathcal{L}_{\mathbf{x}} \mid \mathbf{x} \in \Omega \text{ and } \forall i \in [\![0, q-1]\!],\ \mathbf{x} + \mathbf{v}_i \in \Omega\}$,
- the boundary nodes: $\mathcal{I}_{\mathrm{bd}} = \{\mathbf{x} \in \mathcal{L}_{\mathbf{x}} \mid \mathbf{x} \in \Omega \text{ and } \exists i \in [\![0, q-1]\!],\ \mathbf{x} + \mathbf{v}_i \in \Omega^c\}$,

and the other nodes are not considered. We detail in the following the treatment of nodes belonging to $\mathcal{I}_{\mathrm{in}}$. For the boundary nodes in $\mathcal{I}_{\mathrm{in}}^{\mathrm{bd}}$, many approaches exist depending on the type of boundary condition imposed to the macroscopic fields ρ or $\mathbf{u}$, see [49]. The speed discretized BGK BE (9), written on the space and time lattices reads, for $i \in [\![0, q-1]\!]$, $t \in \mathcal{L}_t$ and $\mathbf{x} \in \mathcal{I}_{\mathrm{in}}$:

$$\frac{\partial a_i}{\partial t}(t,\mathbf{x}) + \mathbf{v}_i \cdot \nabla_{\mathbf{x}} a_i(t,\mathbf{x}) = K_{\mathrm{BGK}}[a_i](t,\mathbf{x}). \tag{24}$$

By using the characteristic method, the equation (24) can be put in the form:

$$a_i(t+\Delta t, \mathbf{x} + \mathbf{v}_i\Delta t) - a_i(t,\mathbf{x}) = \int_t^{t+\Delta t} K_{\mathrm{BGK}}\left[a_i\right](t', \mathbf{x} + \mathbf{v}_i t')\ \mathrm{d}t', \tag{25}$$

and by approximating the integral term using the rectangular rule, the equation (24) takes the following final form, called the discrete Lattice Boltzmann Equations (LBE):

$$a_i(t+\Delta t, \mathbf{x} + \mathbf{v}_i\Delta t) = a_i(t,\mathbf{x}) + \Delta t K_{\mathrm{BGK}}\left[a_i\right](t,\mathbf{x}), \tag{26}$$

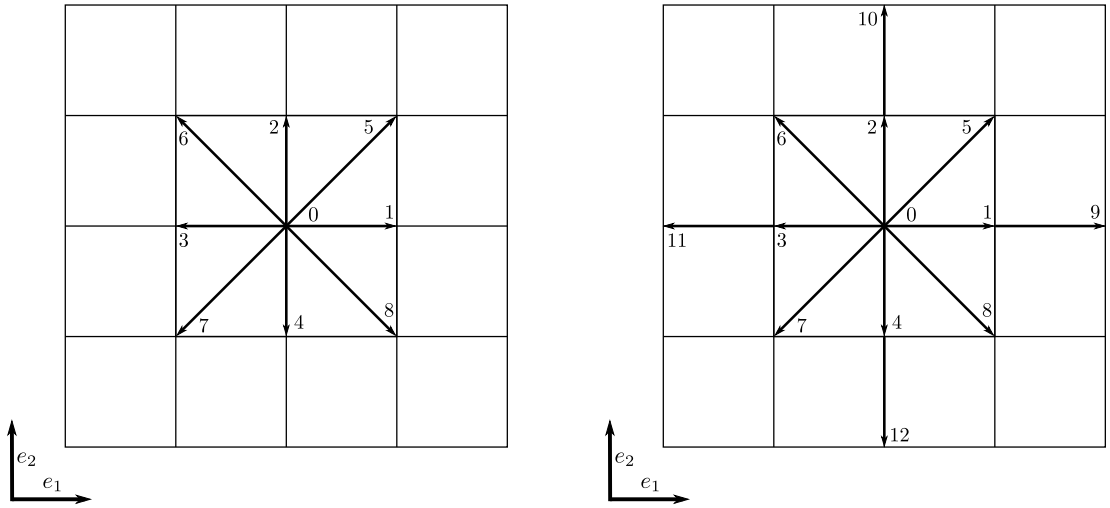

(a) D2Q9 (b) D2Q13

Figure 1: The speed sets D2Q9 in (a) and D2Q13 in (b).

2.6. Solution numerical algorithm

This problem is then solved at each time step following the classical so-called *collide-and-stream* paradigm:

i- the collide step, where each population $a_i(t, \mathbf{x})$ is updated by receiving a local collisional contribution:

$$a_i^*(t, \mathbf{x}) = a_i(t, \mathbf{x}) - \frac{\Delta t}{\tau} \left(a_i(t, \mathbf{x}) - a_i^{\mathrm{eq}}(t, \mathbf{x}) \right), \quad \text{for } i \in [\![0, q-1]\!], \tag{27}$$

ii- the streaming step, where the post collision populations $a_i^*(t, \mathbf{x})$ stream along their associated direction $\mathbf{v}_i$, landing on the corresponding neighbouring lattice site (no particle can fly *off-grid*):

$$a_i(t + \Delta t, \mathbf{x} + \mathbf{v}_i \Delta t) = a_i^*(t, \mathbf{x}), \quad \text{for } i \in [\![0, q-1]\!]. \tag{28}$$

If any, the main *trick* of the LBM lies in the velocity discretization. The advection velocity of BE is the molecules' velocity rather than a mean flow velocity, which leads to constant propagation velocity for each a_i. Through a smart choice of dimensions, each constant $\mathbf{v}_i$ is chosen as to correspond to the grid-spacing to Δt ratio. This yields exact linear advection properties: a_i^* are only moved from one grid point to the next (in the direction of the corresponding discrete velocity) during the streaming step, which is therefore exact and equivalent to only a shift in data tables. Also, as one can see, the collide step is local in space, what ease the use of domain decomposition techniques.

3. The Lattice Boltzmann Method for Radiative Transfer Equation solution

In the previous section we have recalled the main ingredients of the LBM for the NSE. In the following one, we discuss about the LBM adaptation for the RTE. We start by introducing the continuous RTE and the main differences it has with BE. Then we briefly develop the main existing strategies, based on LBM, for its numerical solution and we finish by introducing the principle of the new approach we propose and the advantages it brings.

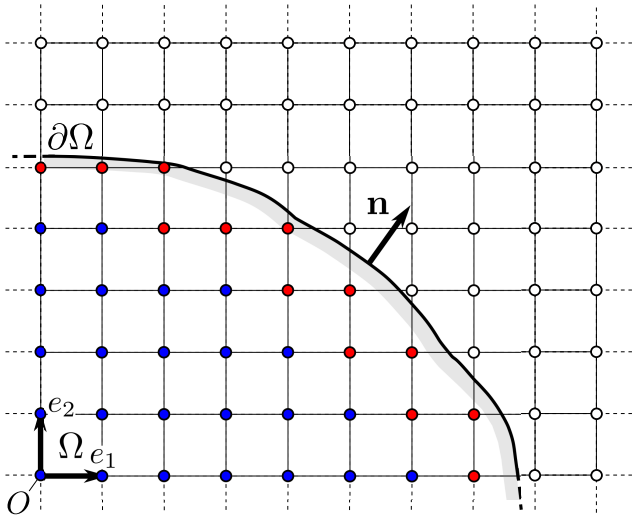

Figure 2: Lattice nodes classification, for $d = 2$, with in blue the nodes of $\mathcal{I}_{\text{in}}$, in red the nodes of $\mathcal{I}_{\text{bd}}$ and in white the nodes that are not considered.

3.1. The Radiative Transfer problem

In this paper, we consider the RTE describing the transport of radiation through a medium, affected only by scattering process. It is an integro-differential equation formulated in terms of an energy density function a. The energy density is a function of $(t, \mathbf{x})$ and also of direction $\hat{\mathbf{k}}$ in the phase domain $I \times \Omega \times \mathbb{S}^{d-1}$. It gives the density of energy which, at t and located at $\mathbf{x}$, has a propagation direction $\hat{\mathbf{k}}$. The RTE reads, $\forall (t, \mathbf{x}, \hat{\mathbf{k}}) \in I \times \Omega \times \mathbb{S}^{d-1}$:

$$\frac{\partial a}{\partial t}(t, \mathbf{x}, \hat{\mathbf{k}}) + v\hat{\mathbf{k}} \cdot \nabla_{\mathbf{x}} a(t, \mathbf{x}, \hat{\mathbf{k}}) = vK[a](t, \mathbf{x}, \hat{\mathbf{k}}), \tag{29}$$

where $v \in \mathbb{R}^*$ is the constant radiation speed propagation. The energy scattering is modelled by $K[a]$, the integral scattering operator, defined as:

$$K[a](t, \mathbf{x}, \hat{\mathbf{k}}) = -\Sigma_t(\mathbf{x})a(t, \mathbf{x}, \hat{\mathbf{k}}) + \Sigma_s(\mathbf{x}) \int_{\mathbb{S}^{d-1}} \sigma(\hat{\mathbf{k}} \cdot \hat{\mathbf{k}}')a(t, \mathbf{x}, \hat{\mathbf{k}}') \, \mathrm{d}\hat{\mathbf{k}}' \tag{30}$$

where Σ_t is the total scattering coefficient, equal to the sum of Σ_s, the scattering cross section and $\Sigma_a$the absorption coefficient which are physical parameters of the medium ($\Sigma_t = \Sigma_s + \Sigma_a$). The scattering phase function σ gives the energy fraction propagating in direction $\hat{\mathbf{k}}'$ deviated in the direction $\hat{\mathbf{k}}$. For the sake of clarity, we omit to write the dependence of σ on $\mathbf{x}$, as it has no influence on the development of the method. It is normalized as:

$$\int_{\mathbb{S}^{d-1}} \sigma(\hat{\mathbf{k}} \cdot \hat{\mathbf{k}}') \, \mathrm{d}\hat{\mathbf{k}}' = 1. \tag{31}$$

We also define the total energy E and the radiative flux $\mathbf{F}$ as the zeroth and first order moments of a, respectively, i.e.:

$$E(t, \mathbf{x}) = \int_{\mathbb{S}^{d-1}} a(t, \mathbf{x}, \mathbf{k}') \, \mathrm{d}\mathbf{k}', \text{ and } \mathbf{F}(t, \mathbf{x}) = \int_{\mathbb{S}^{d-1}} \mathbf{k}' a(t, \mathbf{x}, \mathbf{k}') \, \mathrm{d}\mathbf{k}'. \tag{32}$$

In order to formulate a complete RT problem, we add to equation (29) an initial condition that reads:

$$a(0, \mathbf{x}, \hat{\mathbf{k}}) = a_0(\mathbf{x}, \hat{\mathbf{k}}), \ \forall (\mathbf{x}, \hat{\mathbf{k}}) \in \Omega \times \mathbb{S}^{d-1}, \tag{33}$$

where a_0 is a given field, as well as a Dirichlet boundary condition:

$$a(t, \mathbf{x}, \hat{\mathbf{k}}) = a_d(t, \mathbf{x}, \hat{\mathbf{k}}),\ \forall (t, \mathbf{x}, \hat{\mathbf{k}}) \in I \times \Gamma^-_{\hat{\mathbf{k}}} \times \mathbb{S}^{d-1}, \tag{34}$$

where a_d a given field and $\Gamma^-_{\hat{\mathbf{k}}}$ is the incoming boundary for a given direction $\hat{\mathbf{k}}$. It is a portion of $\partial\Omega$, defined as:

$$\Gamma^-_{\hat{\mathbf{k}}} = \left\{ \mathbf{x} \in \partial\Omega \mid \mathbf{n}(\mathbf{x}) \cdot \hat{\mathbf{k}} < 0 \right\}, \tag{35}$$

with $\mathbf{n}$ the unit outward normal vector to $\partial\Omega$. This boundary condition corresponds to totally transparent wall, see [2] for other types of boundary conditions.
As one can see, the following formulation of the RTE (equation (29)) differs from the BE (equation (9)) used in the LBM mainly by the fact that the velocity field in the advection operator is not the distribution function speed variable $\mathbf{v}$, which lives in $\mathbb{R}^d$, but a field $v\hat{\mathbf{k}}$, depending on the direction of energy propagation, which lives on a $(d-1)$-sphere. In fact, the RTE we use is equivalent to a mono-kinetic BE, i.e. where particles move at speed $\mathbf{v} = v\hat{\mathbf{k}}$ and then where the particle density function a depends only on $(t, \mathbf{x}, \hat{\mathbf{k}})$. This small difference leads, if one uses the characteristic method with a regular space and time lattices, as done in the LBM and recalled in subsections 2.3 and 2.6, to *off-grid* propagation.

3.2. Brief overview of existing strategies based on LBM

Several approaches have been developed to use or adapt the LBM for the RTE solution to take advantage of its effectiveness, we classify them into three categories.
A first category of approaches aims to solve an approximated version of the RTE, called the P_1 approximation (see the book [2, Chapter 16] for more details on the P_N approximation of the RTE). In this case, the energy density takes the following form:

$$a(t, \mathbf{x}, \hat{\mathbf{k}}) \approx \frac{1}{4\pi} E(t, \mathbf{x}) + \frac{3}{4\pi} \mathbf{F}(t, \mathbf{x}) \cdot \hat{\mathbf{k}}. \tag{36}$$

Also, considering the highly scattering regime, i.e. $\Sigma_a \ll \Sigma_s$, homogeneous Σ_a and Σ_s coefficients and assuming the steady state is reached instantaneously, the following macroscopic steady diffusion equation is classically used (see e.g. [51]):

$$\frac{1}{3(\Sigma_a + \Sigma_s)} \Delta E = \Sigma_a E. \tag{37}$$

Many works have used the LBM to solve equation (37), considering it as the macroscopic targeted model, see [36–38] or [39] and the references therein and [40] for a rigorous established link between the adapted LBM and the macroscopic model, using the Chapman-Enskog expansion mentioned in subsection 2.4.
A second category, initially developed by [41] for the steady RTE and later in [42] and [8] for the unsteady RTE aims to solve the system of coupled convection equations arising from the discretization in direction of the RTE by means of the DOM (or S_N-approximation). The DOM relies on the discretization of the angular domain $\mathbb{S}^{d-1}$ by the introduction of N discrete directions and the construction of an associated quadrature method to approximate the integral terms. Several sets of directions $\hat{\mathbf{k}}_i$ and weights w_i exist, constructed from different constrains (see e.g. [2, Chapter 17] of [52, 53] for more details). Then the integral scattering term is approximated using the quadrature and the equation (29) is replaced by a system of N coupled equations of N unknowns, corresponding to the energy density evaluation at the discrete directions. To solve this system of equations, the authors use the LBM as a direct numerical solver by adapting the developments realized for the general case of convection-diffusion equations, as for example the works of the paper [43] (which extends

those of [44]), to their particular case. It consists in solving the system of N coupled equations by introducing for each unknown a_i a set of q distribution functions and using a LBM scheme. The major drawback of this approach is that it becomes very heavy from a memory point of view because $N \times q$ unknown fields, depending on time and space, are introduced.
The last category of method is the one recently proposed by [45]. In their approach the authors start by approximating the energy density with respect to its dependence on the direction by projecting it on the spherical harmonics (see e.g. the book [54, Chapter 4] for more information about spherical harmonics approximation theory). They consider several quadratures, constructed such that it integrates exactly all the spherical harmonics up to a given degree. In Figure 3 is depicted an example of a uniformly spaced direction set the authors used, for the case $d = 2$, with $N = 12$ directions given by $\hat{\mathbf{k}}_i = (\cos(\psi_i), \sin(\psi_i))$ with $\psi_i = 2\pi(i-1)/N$ and with the associate weights $w_i = 1/N$. Then, the authors fully discretized the RTE by using the same classical procedure used for the BE in the LBM framework we detailed in subsection 2.5. As the Figure 3 shows, even if we set $\Delta x = v\Delta t$, the energy density will propagate *off-grid* in some directions. To overcome this difficulty, the authors propose to use a spatial d-interpolation scheme. A drawback of this approach is that d-interpolation is numerically expensive and may introduce spatial diffusion of the energy.

directly the steady or unsteady RTE, with principally two types of methods. A first type of methods, starts by approximating the RTE

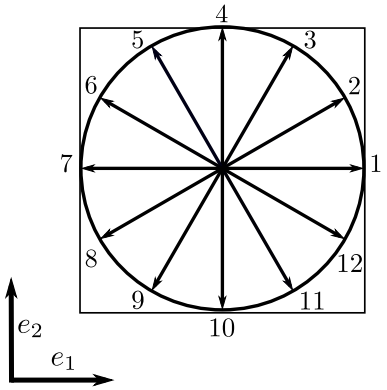

Figure 3: Example of a uniformly spaced direction set used in [45] in the case where $d = 2$, $N = 12$ and $\Delta x = v\Delta t$.

3.3. Interest of multiple time steps for LBM-based RTE

In this work, we propose an alternative approach to the spatial d-interpolation scheme proposed by [45], aiming to conserve an *on-grid* streaming. It is based on the use of a particular $(d-1)$-sphere discretization, considering only directions which link lattice nodes, i.e. directions of space $\mathcal{D}$ defined as:

$$\mathcal{D} = \left\{ \frac{\mathbf{z}}{\|\mathbf{z}\|} \in \mathbb{S}^{d-1} \mid \mathbf{z} \in \mathbb{Z}^d \backslash \left\{ \mathbf{0}^d \right\} \right\} \tag{38}$$

(where $\mathbf{0}^d$ is the null vector of $\mathbb{Z}^d$), as well as the construction of a quadrature. This discretization, by defining for each directions a particular time discretization with a specific step, allows to recover an *on-grid* streaming. The difficulty arising with this approach is to manage the several time discretizations introduced which may be incompatible. To overcome it, we propose to treat the incompatibilities by a time linear interpolation. We detail in what follows the whole procedure.

4. A Staggered Lattice Boltzmann Method for the Radiative Transfer problem

In the previous sections we have recalled the main ingredients of the LBM, introduced the continuous RTE and discussed its main differences with the BE. We have briefly presented the different existing strategies which are based on LBM to solve the RTE.
In this section we present in details the Staggered Lattice Boltzmann Method for the RTE we propose. This method aims at conserving an *on-grid* streaming while using some of the LBM ingredients. The *on-grid* property being relative to a spatial discretization, we discretize the space $\mathbb{R}^d$ by introducing a d-dimensional lattice denoted $\mathcal{L}_{\mathbf{x}} = \Delta x \times \mathbb{Z}^d$ of constant step $\Delta x > 0$ in the d directions.

4.1. Discretization in direction space

As done classically for the numerical solution of the RTE (see subsection 3.2), we discretize the directions space $\mathbb{S}^{d-1}$. However, to ensure *on-grid* streaming, not all points from $\mathbb{S}^{d-1}$ can be considered but only those that belong to $\mathcal{D}$ (see equation (38)). We group all the vectors of $\mathbb{Z}^d \backslash \{\mathbf{0}^d\}$ by their euclidian norms in an infinite collection of sets $\{\mathcal{Z}_i,\ i \in \mathbb{N}^\star\}$ and normalize them. These sets are indexed on $\mathbb{N}^*$ in ascending order of norm:

$$\mathcal{Z}_i = \left\{ \frac{\mathbf{z}}{\|\mathbf{z}\|} \in \mathbb{S}^{d-1} \mid \mathbf{z} \in \mathbb{Z}^d \text{ and } \|\mathbf{z}\| = c_i \right\} \subset \mathcal{D} \quad \forall i \in \mathbb{N}^\star, \tag{39}$$

with $c_i \in \mathbb{R}_+^\star$ the $\mathcal{Z}_i$ associated norm (with $c_i \leqslant c_j$ if $i \leqslant j$). Then we proceed recursively as follows:

- Initialization ($k = 1$): we define the first set of directions $\mathcal{S}_1$:

$$\mathcal{S}_1 = \{\mathbf{v}_i = \mathbf{e}_i \text{ for } i \in [\![1, d]\!]\} \, (= \mathcal{Z}_1)\,. \tag{40}$$

- Inductive step ($k > 1$): we define the k-th set of directions $\mathcal{S}_k$:

$$\mathcal{S}_k = \mathcal{Z}_k \backslash (\mathcal{S}_1 \cup \cdots \cup \mathcal{S}_{k-1}) \tag{41}$$

  to ensure that no direction is considered several times. The number of direction of $\mathcal{S}_k$ will be denoted N^k.

As an example, the first four sets for the case $d = 2$ are given in Table 1 and represented in Figure 4.
Then, we choose $N_{\mathcal{S}}$ directions sets, whose set of indexes is denoted $I \subset \mathbb{N}^\star$. In the following, we will denote by I_n, with $n \in [\![1, N_{\mathcal{S}}]\!]$, an element of I and $\hat{\mathbf{k}}_i^n$, with $i \in [\![1, N^{I_n}]\!]$ the directions of $\mathcal{S}_{I_n}$.
Now we have constructed a direction discretization, we use specific quadratures to approximate the integral terms. Thus, for each discrete direction $\hat{\mathbf{k}}_j^m$ with $n \in [\![1, N_{\mathcal{S}}]\!]$ and $i \in [\![1, N^{I_n}]\!]$ we write:

$$\int_{\mathbb{S}^{d-1}} \sigma(\hat{\mathbf{k}}_i^n \cdot \hat{\mathbf{k}}') a(t, \mathbf{x}, \hat{\mathbf{k}}') \, \mathrm{d}\hat{\mathbf{k}}' \approx \sum_{m=1}^{N_{\mathcal{S}}} \sum_{j=1}^{N^{I_m}} w_{ij}^{nm} a(t, \mathbf{x}, \hat{\mathbf{k}}_j^m), \tag{42}$$

with $w_{ij}^{nm} > 0$ the weight associated to the direction $\hat{\mathbf{k}}_j^m$. The way we define the weights, following the principle of the DOM, is explained in the Appendix A. We define the approximated integral scattering operator by:

$$\tilde{K}[a](t,\mathbf{x},\hat{\mathbf{k}}_i^n) = -\Sigma_t(\mathbf{x})a(t,\mathbf{x},\hat{\mathbf{k}}_i^n) + \Sigma_s(\mathbf{x})\sum_{m=1}^{N_{\mathcal{S}}}\sum_{j=1}^{N^{I_m}} w_{ij}^{nm} a(t,\mathbf{x},\hat{\mathbf{k}}_j^m). \tag{43}$$

We construct also a quadrature to approximate the energy density zeroth and first order moments by following the same approach:

$$E(t,\mathbf{x}) \approx \sum_{n=1}^{N_{\mathcal{S}}}\sum_{i=1}^{N^{I_n}} w_i^n a(t,\mathbf{x},\hat{\mathbf{k}}_i^n) \text{ and } \mathbf{F}(t,\mathbf{x}) \approx \sum_{i=1}^{N^{I_n}} w_i^n \hat{\mathbf{k}}_i^n a(t,\mathbf{x},\hat{\mathbf{k}}_i^n) \tag{44}$$

with $w_i^n > 0$ the weight associated to the direction $\hat{\mathbf{k}}_i^n$.
Before to give the discrete in space-direction RT problem, we separate the nodes of the spatial lattice $\mathcal{I}$ into two sets, the internal nodes and border ones. However this two sets definition will depend on the considered direction propagation. Thus, for each $n \in [\![1, N_{\mathcal{S}}]\!]$ and $i \in [\![1, N^{I_n}]\!]$, we define:

- the internal nodes: $\mathcal{I}_{\text{in}}^{n,i} = \left\{\mathbf{x} \in \mathcal{L}_{\mathbf{x}} \mid \mathbf{x} \in \Omega \text{ and } \mathbf{x} - v\hat{\mathbf{k}}_i^n \Delta t_n \in \Omega\right\}$,
- the boundary nodes: $\mathcal{I}_{\text{bd}}^{n,i} = \left\{\mathbf{x} \in \mathcal{L}_{\mathbf{x}} \mid \mathbf{x} \in \Omega \text{ and } \mathbf{x} - v\hat{\mathbf{k}}_i^n \Delta t_n \in \Omega^c\right\}$,

and the other nodes are not considered. The discrete in space-direction RT problem reads:

For each $n \in [\![1, N_{\mathcal{S}}]\!]$, $i \in [\![1, N^{I_n}]\!]$, find a_i^n such that, $\forall t \in I$ we have:

$$\frac{\partial a_i^n}{\partial t}(t,\mathbf{x}) + v\hat{\mathbf{k}}_i^n \cdot \nabla_{\mathbf{x}} a_i^n(t,\mathbf{x}) = v\tilde{K}[a](t,\mathbf{x},\hat{\mathbf{k}}_i^n), \quad \forall \mathbf{x} \in \mathcal{I}_{\text{in}}^{n,i}, \tag{45}$$

$$a_i^n(0,\mathbf{x}) = \frac{1}{w_i^n} a_0(\mathbf{x},\hat{\mathbf{k}}_i^n), \quad \forall \mathbf{x} \in \Omega, \tag{46}$$

$$a_i^n(t,\mathbf{x}) = \begin{cases} \dfrac{1}{w_i^n} a_d(t,\mathbf{x},\hat{\mathbf{k}}_i^n) & \text{if } \hat{\mathbf{k}}_i^n \cdot \mathbf{n} \leqslant 0, \\ 0 & \text{else,} \end{cases} \quad \forall \mathbf{x} \in \mathcal{I}_{\text{bd}}^{n,i} \tag{47}$$

where, for the sake of clarity, $a_i^n(t,\mathbf{x}) = a(t,\mathbf{x},\hat{\mathbf{k}}_i^n)$.

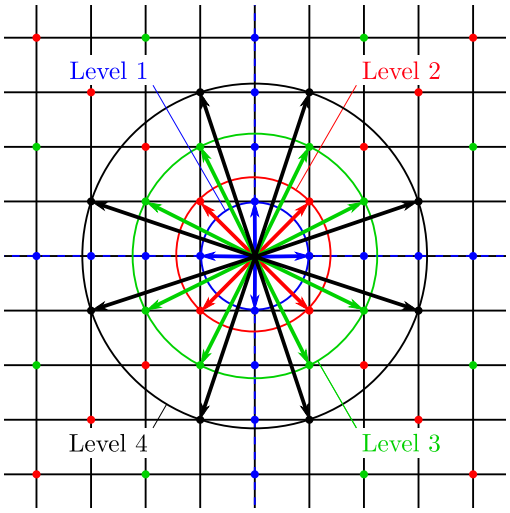

Figure 4: The first four direction sets $\mathcal{S}_k$ in the case of $d = 2$.

k	c_k	$\mathcal{S}_k$	N^k	Color on Fig. 4
1	1	$\{(1,0),(0,1),(-1,0),(0,-1)\}$	4	Blue
2	$\sqrt{2}$	$\{(1,1),(-1,1),(-1,-1),(1,-1)\}$	4	Red
3	$\sqrt{5}$	$\{(2,1),(-1,2),(-2,-1),(1,-2),$ $(1,2),(-2,1),(-1,-2),(2,-1)\}$	8	Green
4	$\sqrt{10}$	$\{(3,1),(-1,3),(-3,-1),(1,-3),$ $(1,3),(-3,1),(-1,-3),(3,-1)\}$	8	Black

Table 1: The first four directions sets $\mathcal{S}_k$ in the case of $d = 2$.

4.2. Time discretization

We introduce, for each chosen direction set $\mathcal{S}_n$ ($n \in [\![1, N_{\mathcal{S}}]\!]$), a 1-dimensional time lattice $\mathcal{L}_t^n = \Delta t_n \times]\!]0, N_t^n]\!]$ of constant step $\Delta t_n > 0$ such that: $\Delta t_n = \Delta t \times c_n$ with $\Delta t = \Delta x/v$ and $\mathcal{L}_t^n$ fully overlaps I, see Figure 5. In the following we will denote the discrete instant of each time lattice: $t_l^n = l \times \Delta t_n$ for $l \in]\!]0, N_t^n]\!]$.
We use for each equation of the system (45), as done in LBM, the characteristic method as well as the rectangular rule with the associated time discretization. We then obtain the following fully discrete RT problem:

For each $n \in [\![1, N_{\mathcal{S}}]\!]$, $i \in [\![1, N^{I_n}]\!]$, find a_i^n such that, $\forall t_l^n \in \mathcal{L}_t^n$ we have:

$$a_i^n(t_{l+1}^n, \mathbf{x} + v\hat{\mathbf{k}}_i^n \Delta t_n) = a_i^n(t_l^n, \mathbf{x}) + v\Delta t_n \tilde{K}[a](t_l^n, \mathbf{x}, \hat{\mathbf{k}}_i^n), \quad \text{for } \mathbf{x} \in \mathcal{I}_{\text{in}}^{n,i}, \tag{48}$$

$$a_i^n(0, \mathbf{x}) = \frac{1}{w_i^n} a_0(\mathbf{x}, \hat{\mathbf{k}}_i^n), \quad \forall \mathbf{x} \in \Omega, \tag{49}$$

$$a_i^n(t_{l+1}^n, \mathbf{x}) = \begin{cases} \dfrac{1}{w_i^n} a_d(t_{l+1}^n, \mathbf{x}, \hat{\mathbf{k}}_i^n) & \text{if } \hat{\mathbf{k}}_i^n \cdot \mathbf{n} \leqslant 0, \\ 0 & \text{else,} \end{cases} \quad \text{for } \mathbf{x} \in \mathcal{I}_{\text{bd}}^{n,i}. \tag{50}$$

As one can see, according to equation (48), we need to compute the term $\tilde{K}[a](t_l^n, \mathbf{x}, \hat{\mathbf{k}}_i^n)$ at t_l^n to obtain the a_i^n at t_{l+1}^n. To do so, all a_i^n need to be known at the considered instant, which is not a priori the case because the different time lattices are not necessary compatible. We detail in the following subsection how we numerically overcome this difficulty.

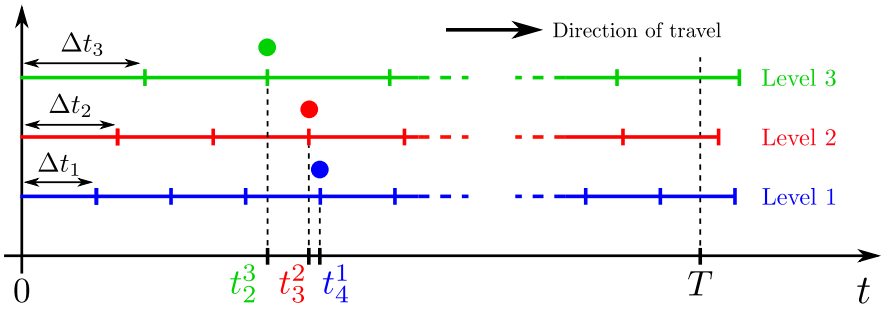

Figure 5: Diagram representing three different time lattices. The three circles indicate the traversal position of each time lattice.

4.3. Solution numerical algorithm

To overcome the difficulty coming from the time lattices incompatibilities and to avoid a long and memory consuming construction of a global time lattice, obtained by the computing

of all the intersections between the different time lattices, we introduce a traversal algorithm. It consists in the following steps:

1. Initialization:
   (a) We introduce a vector of $N_{\mathcal{S}}$ components, denoted by $\mathbf{s}$, giving the traversal position of each time lattice. We initialize it full of zeros: $\mathbf{s}_n = 0$ for $n \in [\![1, N_{\mathcal{S}}]\!]$.
   (b) We initialize the $\sum_{n=1}^{N_s} N^{I_n}$ distribution functions: $a_i^n(0, \mathbf{x}) = a_0(\mathbf{x}, \hat{\mathbf{k}}_i^n),\ \forall \mathbf{x} \in \mathcal{I}_{\text{in}}^{n,i}$.
   (c) We compute $\tilde{K}[a](0, \mathbf{x}, \hat{\mathbf{k}}_i^n)$ using equation (43).
   (d) For all direction sets, i.e. $n \in [\![1, N_{\mathcal{S}}]\!]$, we solve the problem (48) using the *collide-and-stream* paradigm of the LBM and obtain the value of all energy densities: $a_i^n(t_1^n, \mathbf{x}),\ \forall \mathbf{x} \in \mathcal{I}_{\text{in}}^{n,i}$.
2. Current step: while all the time lattices have not been traversed, i.e. while $\mathbf{s}_n < N_t^n$ for $n \in [\![1, N_{\mathcal{S}}]\!]$.
   (a) We search which time lattices have the least advances traversing, by determining t_c the lowest time such that: $t_c = \min\left(\left\{t_{\mathbf{s}_n}^n,\ n \in [\![1, N_{\mathcal{S}}]\!]\right\}\right)$ and regrouping the number of these lattices in a set $\mathcal{C} = \left\{n \mid t_{\mathbf{s}_n}^n = t_c\right\}$. We denote $\mathcal{C}^c = [\![1, N_{\mathcal{S}}]\!] \backslash \mathcal{C}$. For example on Figure 5, where three direction sets are considered, $t_c = t_2^3$ and only the third time lattice has been traveled exactly up to this point so $\mathcal{C} = \{3\}$ and $\mathcal{C}^c = \{1, 2\}$.
   (b) To compute $K[a](t_c, \mathbf{x}, \hat{\mathbf{k}}_i^n)$ we need to know the energy distribution values of time lattices which belong to $\mathcal{C}^c$ at t_c. Since their values are known at times $t_{\mathbf{s}_n}^n > t_c$ and $t_{\mathbf{s}_n-1}^n < t_c$, we do a linear interpolation:
   $$a_i^n(t_c, \mathbf{x}) = \frac{t_{\mathbf{s}_n}^n - t_c}{\Delta t_n} a_i^n(t_{\mathbf{s}_n-1}^n, \mathbf{x}) + \frac{t_c - t_{\mathbf{s}_n-1}^n}{\Delta t_n} a_i^n(t_{\mathbf{s}_n}^n, \mathbf{x}), \quad \text{for } n \in \mathcal{C}^c,\ i \in [\![1, N^{I_n}]\!] \text{ and } \mathbf{x} \in \mathcal{I}_{\text{in}}^{n,i}. \tag{51}$$
   (c) We compute $K[a](t_c, \mathbf{x}, \hat{\mathbf{k}}_i^{I_n})$ using equation (43).
   (d) For each $n \in \mathcal{C}$, we solve the problem (48) using the *collide-and-stream* paradigm of the LBM and obtain the value of all energy densities: $a_i^n(t_{j+1}^n, \mathbf{x}),\ \forall \mathbf{x} \in \mathcal{I}_{\text{in}}^{n,i}$.
   (e) We update the state vector by incrementing each component belonging to $\mathcal{C}$ ($\mathbf{s}_n = \mathbf{s}_n + 1$ with a computer writing).

The treatment of the boundary nodes is realized at the step (1d) of initialization and step (2d) of the loop, during the streaming step. As discussed in subsubsection 4.1, the boundary nodes depend on the considered propagating direction with the definition of $\mathcal{I}_{\text{bd}}^{n,i}$. To verify the boundary condition given by equation (34), we impose, for each $n \in [\![1, N_{\mathcal{S}}]\!]$ and $i \in [\![1, N^{I_n}]\!]$ during initialization and for each $n \in \mathcal{C}$ and $i \in [\![1, N^{I_n}]\!]$ during the loop the equation (50). As one can see, the fact of using a time interpolation instead of a space one has the advantage to only use data at the same node and therefore recovers the local aspect of the LBM. On the other hand this is paid by an increase in the total number of time steps compared to an approach with one time discretization and also the need to keep the a_i values at two consecutive time steps. Thus, the memory footprint is (only) double (so same order of magnitude) that for the classical LBM.
Now we have presented the different ingredients of the Staggered Lattice Boltzmann Method we propose for the RTE, we demonstrate its relevance and potential, in the next section, through several two-dimensional numerical tests.

5. Numerical examples

In this section we apply our approach to several two-dimensional ($d = 2$) problems taken from literature. We consider only direction sets of the form: $\mathcal{D}_{N_\mathcal{S}} = \bigcup_{k=1}^{N_\mathcal{S}} \mathcal{S}_k$, i.e. the set containing the indexes of chosen sets $\mathcal{S}_k$ is of the form: $I = [\![1, N_\mathcal{S}]\!]$.

5.1. A laser problem

The first problem we consider is extracted from [45]. It consists in the modeling of the streaming of a radiation beam, injected from a part of the boundary, denoted Γ_i, of a square-shaped domain of side l: $\Omega =]0, l[\times]0, l[$, in a direction $\mathbf{e}_{\text{las}}$ (assuming that $\mathbf{e}_{\text{las}} \cdot \mathbf{n} \leqslant 0$ on Γ_i), over I (see Figure 6). We assume that the medium in which the laser streams does not absorb neither scatter radiations, i.e. $\Sigma_a = \Sigma_s = 0$, so that the RTE simplifies to a free transport equation. We then consider two different cases. In both the function a_d of the boundary condition is given by:

$$a_d(t, \mathbf{x}_d, \hat{\mathbf{k}}) = \mathbf{1}_{\Gamma_i}(\mathbf{x}_d)\delta(\hat{\mathbf{k}} - \mathbf{e}_{\text{las}}) \tag{52}$$

with $\mathbf{1}_{\Gamma_i}$ the indicator function of Γ_i and δ the Dirac distribution. For the numerical application we have considered the following parameters without dimension: $v = 1$, $l = 1$ and $T = 1$. To make comparisons, we have used the space interpolation approach proposed in [45] with:

- a 2-dimensional lattice $\mathcal{L}_\mathbf{x}$, covering Ω with a constant step $\Delta x = 1/200$,
- a 1-dimensional lattice $\mathcal{L}_t$, covering I with a constant step $\Delta t = \Delta x/v = 1/200$,
- a set of 8 uniformly spaced directions: $\left\{\hat{\mathbf{k}}_i = [\cos(\phi_i), \sin(\phi_i)] \mid \phi_i = 2\pi i/8,\ i \in [\![1, 8]\!]\right\}$ all with the same quadrature weight $w_i = 1/8$,

and the SLBM approach with:

- the same 2-dimensional lattice $\mathcal{L}_\mathbf{x}$,
- a direction set $\mathcal{D}_2$ ($= \mathcal{S}_1 \cup \mathcal{S}_2$ as defined in subsubsection 4.1), with also 8 directions and quadrature weights as constructed in Appendix A,
- the 1-dimensional lattices associated to each direction sets ($\mathcal{L}_t^1 = \mathcal{L}_t$ with $\Delta t_1 = \Delta t$, for $\mathcal{S}_1$ and $\mathcal{L}_t^2$ with $\Delta t_2 = \sqrt{2}\Delta t$ for $\mathcal{S}_2$).

Because the problem does not consider scattering and only energy in one direction, the set of directions we have chosen is unnecessarily large but, it allows us to illustrate the effect of the space and time interpolations.

5.1.1. First case

In this case $\Gamma_i = \{0\} \times](l - l_i)/2, (l + l_i)/2[$ with $l_i = 0.5$, $\mathbf{e}_{\text{las}} = \mathbf{e}_1$ and we assume that no energy is initially present in the domain. The geometry of this case is depicted in Figure 6 (a). The initial energy distribution a_0 reads:

$$a_0(\mathbf{x}, \hat{\mathbf{k}}) = 0. \tag{53}$$

The results for the space interpolation approach at two consecutive time steps are given in Figure 7. As expected, the streaming in this case is always *on-grid* and at each time step, the energy value at each point is either 0 or 1. For our SLBM approach, if we only consider

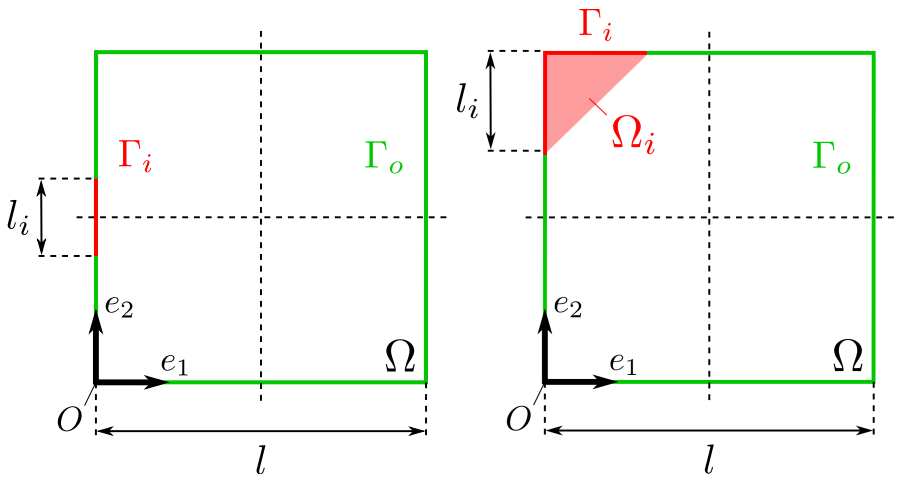

(a) first case. (b) second case.

Figure 6: Geometry of the laser problem for the first case in (a) and the second case in (b).

time belonging to $\mathcal{L}_t^1$, we find back the *on-grid* streaming, as shown by Figures 8 (a), (b) and (d). On the other hand as shown by Figure 8 (c), for time steps belonging to $\mathcal{L}_t^2$, we do not have only values of either 0 or 1, but interpolated values at some lattice nodes. This is best represented in Figure 9. As one can see, because the energy density, propagating in the laser direction, pass from 0 at $t = 0.50$ to 1 at $t = 0.505$ at the nodes in front of the laser, their energy density values are interpolated at $t = 0.502$ to compute the energy density the next time step of $\mathcal{L}_t^2$ at $t = 0.502 + \Delta t_2$.

5.1.2. Second case

In this case $\Gamma_i = \{0\} \times]l - l_i, l[\cup]0, l_i[\times \{l\}$ with $l_i = 0.125$, $\mathbf{e}_{\text{las}} = (\mathbf{e}_1 - \mathbf{e}_2)/\sqrt{2}$ and we assume that initially energy is only present in a sub-domain $\Omega_i = \{\mathbf{x} \in \Omega \mid \mathbf{x} \cdot \mathbf{e}_2 > \mathbf{x} \cdot \mathbf{e}_1 + l - l_i\}$ propagating in the direction $\mathbf{e}_{\text{las}}$. The geometry of this case is depicted in Figure 6 (b). The initial energy distribution a_0 reads:

$$a_0(\mathbf{x}, \hat{\mathbf{k}}) = \mathbf{1}_{\Omega_i}(\mathbf{x}) \delta(\hat{\mathbf{k}} - \mathbf{e}_{\text{las}}). \tag{54}$$

The results are illustrated in Figure 10. As one can see on Figure 10 (a), because the propagating direction fall off lattice nodes, energy density space interpolations are carried out, leading to numerical diffusion. This drawback disappears with our approach as Figure 10 (b) show. This illustrate the main advantage of our approach compared to the space interpolation one. We find of course the same behavior with time interpolations in front of the laser beam as observed with the first case, but at time steps belonging to $\mathcal{L}_t^1$.

5.2. A pulse problem

The third problem is adapted from [8], it consists in studying, over I, a transient radiative transfer in a two-dimensional rectangular-shaped domain of length l_1 and width l_2: $\Omega =]0, l_1[\times]0, l_2[$, induced by submitting its left border, denoted Γ_i, to a short pulse laser irradiation propagating in the direction $\mathbf{e}_1$, see Figure 11. The domain is occupied by an absorbing and isotropically scattering medium, i.e. $\sigma = 1/2\pi$ with a total scattering coefficient $\Sigma_t = 1$. We introduce the scattering albedo ω such that, $\Sigma_s = \omega \times \Sigma_t$. Initially, the domain contains no energy, i.e. the initial energy distribution reads:

$$a_0(\mathbf{x}, \hat{\mathbf{k}}) = 0 \tag{55}$$

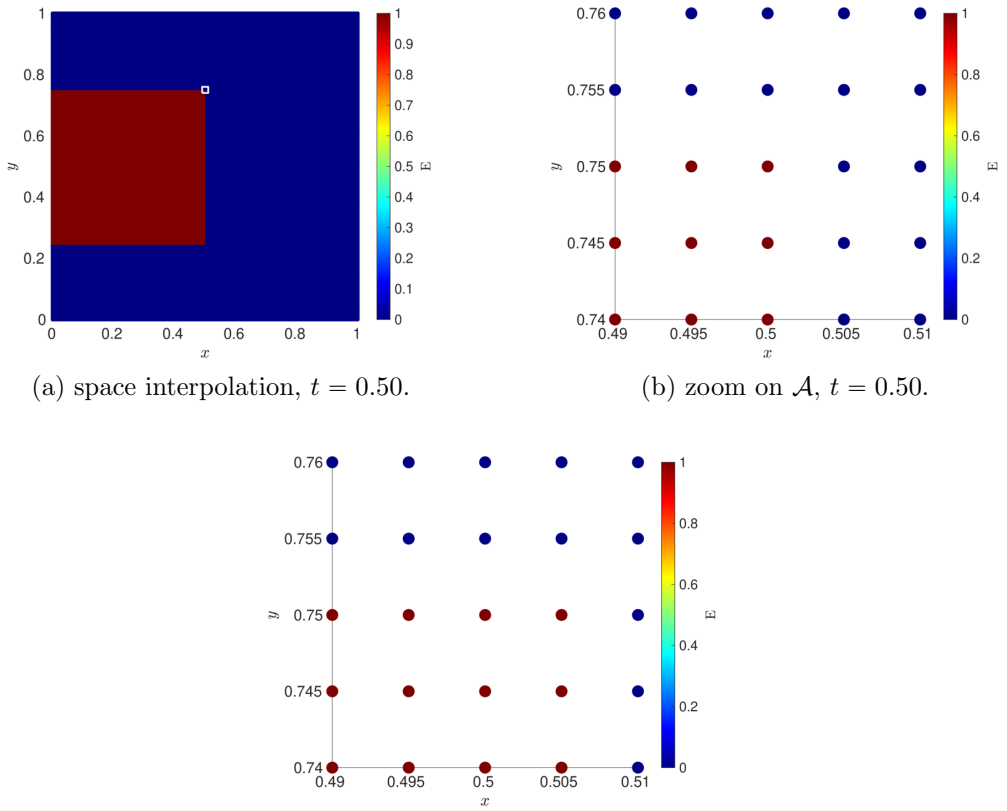

(a) space interpolation, $t = 0.50$.

(b) zoom on $\mathcal{A}$, $t = 0.50$.

(c) zoom on $\mathcal{A}$, $t = 0.505$.

Figure 7: Evolution of the total energy E for the first case with the space interpolation approach at $t = 0.50$ in (a) with a zoom on the area $\mathcal{A} = [0.49, 0.51] \times [0.74, 0.76]$ (represented by a small white contour in (a)) in (b) and the same zoom at $t = 0.50 + \Delta t = 0.505$ in (c).

The square pulse beam is given by:

$$s(t) = s_0 \left[H(t) - H(t - t_p) \right] \tag{56}$$

where H denotes the Heaviside distribution. The medium boundaries are assumed transparent, then the function a_d of the border condition is defined as:

$$a_d(t, \mathbf{x}_d, \hat{\mathbf{k}}) = s(t) \mathbf{1}_{\Gamma_i}(\mathbf{x}_d) \delta(\hat{\mathbf{k}} - \mathbf{e}_1), \quad \forall \mathbf{x}_d \in \Gamma_i \cup \Gamma_o. \tag{57}$$

To simulate an infinite domain in direction $\mathbf{e}_2$, we impose periodic conditions on Γ_p such that:

$$a(t, [x_1, 0], \hat{\mathbf{k}}) = a(t, [x_1, l_2], \hat{\mathbf{k}}), \quad \forall (x_1, \hat{\mathbf{k}}) \in [0, l_1] \times \mathbb{S}^1. \tag{58}$$

To compare our results with the space interpolation approach, we measure two quantities, the reflectance q_r, at point P_r whose coordinates are $\mathbf{x}_r = (0, l_2/2)$, defined by equation (59) and the transmittance q_t, at point P_t whose coordinates are $\mathbf{x}_t = (l_1, l_2/2)$, defined by equation (60).

$$q_r(t) = \frac{1}{s_0} \sum_{n=1}^{N_S} \sum_{\mathbf{n} \cdot \hat{\mathbf{k}}_i^{I_n} > 0} w_i^n \mathbf{n} \cdot \hat{\mathbf{k}}_i^{I_n} a_i^n(t, \mathbf{x}_r) \tag{59}$$

$$q_t(t) = \frac{1}{s_0} \sum_{n=1}^{N_S} \sum_{\mathbf{n} \cdot \hat{\mathbf{k}}_i^{I_n} < 0} w_i^n |\mathbf{n} \cdot \hat{\mathbf{k}}_i^{I_n}| a_i^n(t, \mathbf{x}_t) \tag{60}$$

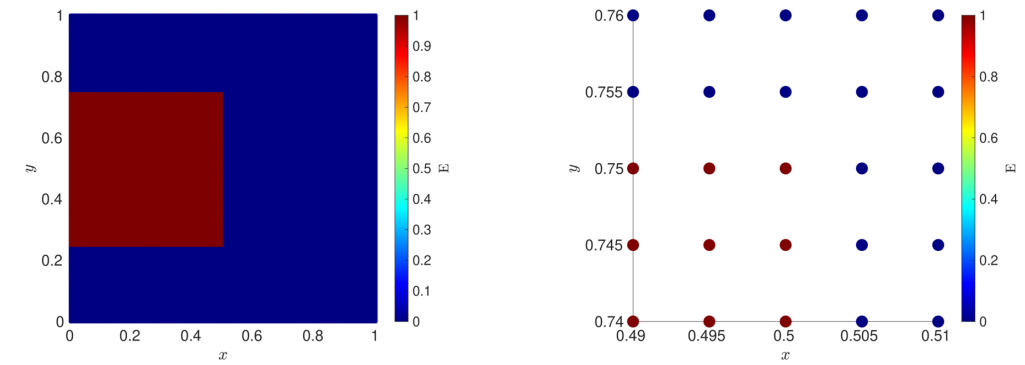

(a) SLBM, $t = 0.50$.

(b) zoom on $\mathcal{A}$, $t = 0.50$.

(c) zoom on $\mathcal{A}$, $t = 0.502$.

(d) zoom on $\mathcal{A}$, $t = 0.505$.

Figure 8: Evolution of the total energy E for the first case with the SLBM approach at $t = 0.50 \in \mathcal{L}_t^1$ in (a) with a zoom on the area $\mathcal{A} = [0.49, 0.51] \times [0.74, 0.76]$ in (b) and the same zoom at $t = 0.502 \in \mathcal{L}_t^2$ in (c) and at $t = 0.50 + \Delta t_1 = 0.505 \in \mathcal{L}_t^1$ in (d).

For the numerical application we have considered the following parameters without dimensions: $v = 1$, $l_1 = 1$, $l_2 = 0.2$, $T = 6$, $t_p = 1$ and $s_0 = 1$. We have used the space interpolation approach with:

- a 2-dimensional lattice $\mathcal{L}_{\mathbf{x}}$, covering Ω with a constant step $\Delta x = 1/500$,
- a 1-dimensional lattice $\mathcal{L}_t$, covering I with a constant step $\Delta t = \Delta x / v = 1/500$,
- a set of 8 uniformly spaced directions $\left\{\hat{\mathbf{k}}_i = [\cos(\phi_i), \sin(\phi_i)] \mid \phi_i = 2\pi i/8, \text{ with } i = 1 \dots 8\right\}$ all with the same quadrature weight $w_i = 1/8$,

and the SLBM approach with:

- the same 2-dimensional lattice $\mathcal{L}_{\mathbf{x}}$,
- the direction set $\mathcal{D}_2$ and quadrature weights as construted in Appendix A.
- the 1-dimensional lattices associated to each subsets of $\mathcal{D}_2$.

The reflectance and transmittance evolution over I we obtain, with an albedo $\omega = 1.0$, are depicted in Figure 12. As one can see, the SLBM and space interpolation approaches give really close results. On Figure 12 (c), we can see that the space interpolation approach, because of the numerical space diffusion, the transmittance evolution is slightly smoothed

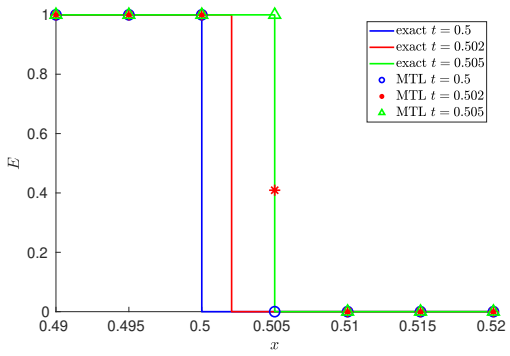

Figure 9: Evolution of the exact total energy E and the one obtained with the SLBM approach, for the first case, at nodes of $\mathcal{L}_{\mathbf{x}}$ belonging to the segment $[0.49, 0.52] \times \{0\}$ at $t = 0.50$, $t = 0.502$ and $t = 0.505$.

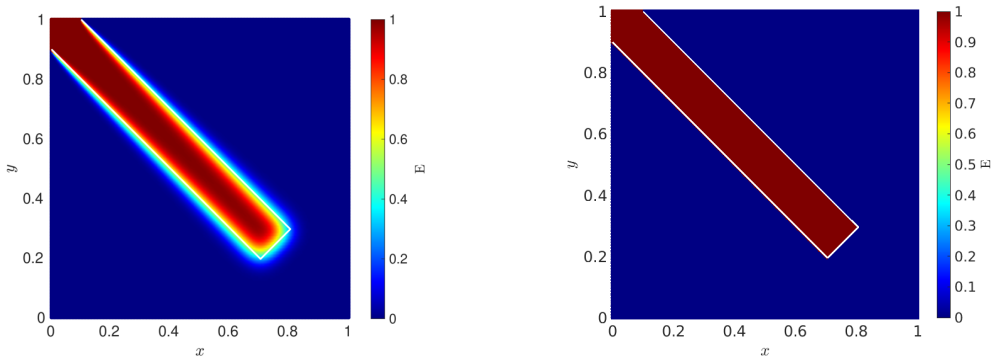

(a) space interpolation, $t = 0.9970$.

(b) SLBM, $t = 0.997$.

Figure 10: Evolution of the total energy E for the second case with the space interpolation approach at $t = 0.9970$ in (a) and with the SLBM approach at $t = 0.9970$ in (b). The exactly streamed beam is represented by a white contour in (a) and (b).

and its values in the upper part are moderately lower. Of course none of these solutions can be considered as the problem exact solution.

The results we obtain with others albedo values are depicted in Figure 13. As observed in [8], we see that an increase of scattering albedo leads to an increase in both the reflectance and transmittance.

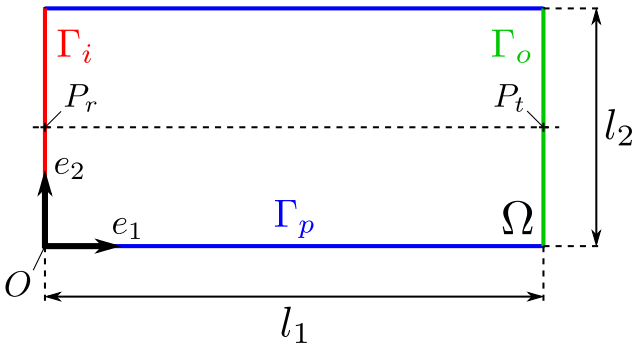

Figure 11: Geometry of the pulse problem.

5.3. Anisotropic and inhomogeneous problem

The last problem we consider is taken form [27]. It consists in the streaming of a radiation beam, injected from a part of the boundary, denoted Γ_i, of a square-shaped domain of length l: $\Omega =]-l/2, l/2[\times]-l/2, l/2[$, in the direction $\mathbf{e}_1$, over I, see Figure 14. The domain is occupied by an heterogeneous, absorbing and anisotropically scattering medium with $\Sigma_a = 0.01$, a scattering coefficient Σ_s which is equal to 1 throughout the domain, except in the interior of a circle of radius 0.3 centered at P_c whose coordinates are $\mathbf{x}_c = (1, 1.5)$ where Σ_s is equal to 5. Thus:

$$\Sigma_s(\mathbf{x}) = \begin{cases} 1 & \text{if } \|\mathbf{x} - \mathbf{x}_c\| > 0.3, \\ 5 & \text{if } \|\mathbf{x} - \mathbf{x}_c\| \leqslant 0.3. \end{cases} \tag{61}$$

The anisotropic scattering is represented by the Henyey–Greenstein phase function (see [55]) which in two dimension is given by:

$$f(\hat{\mathbf{k}} \cdot \hat{\mathbf{k}}') = \frac{1}{2\pi} \frac{1 - g^2}{1 + g^2 - 2g\cos(\hat{\mathbf{k}} \cdot \hat{\mathbf{k}}')} \tag{62}$$

where g is the mean cosine scattering angle or anisotropy factor (the scattering is isotropic for $g = 0$, and becomes more and more sharply peaked in the forward direction as g tend to 1). For this application we take $g = 0.7$. Initially, the domain contains no energy, i.e. the initial energy distribution reads:

$$a_0(\mathbf{x}, \hat{\mathbf{k}}) = 0 \quad \forall (\mathbf{x}, \hat{\mathbf{k}}) \in \Omega \times \mathbb{S}^1. \tag{63}$$

The beam profile is given by:

$$s_p(t, \mathbf{x}_d) = f(t) f(\mathbf{x}_d) \quad \forall \mathbf{x}_d \in \Gamma_i \tag{64}$$

where:

$$f(t) = \frac{2}{\pi} \exp\left[-\left(\frac{t - t_0}{\sigma_t} \right)^2 \right] \text{ and } f(\mathbf{x}_d) = \exp\left[-\left(\frac{\|\mathbf{x}_d - \mathbf{x}_l\|}{\sigma_s} \right)^2 \right] \tag{65}$$

with the standard deviation $\sigma_t = 1/\sqrt{2}$, $\sigma_s = 1/\sqrt{10}$, $t_0 = 1$ and $\mathbf{x}_l = (-2.5, 1.5)$. The medium boundaries are assumed transparent, then the function a_d of the border condition is defined as: $\forall \mathbf{x}_d \in \Gamma_i \cup \Gamma_o$

$$a_d(t, \mathbf{x}_d, \hat{\mathbf{k}}) = s_p(t, \mathbf{x}_d) \mathbf{1}_{\Gamma_i}(\mathbf{x}_d) \delta(\hat{\mathbf{k}} - \mathbf{e}_1) \tag{66}$$

For the numerical application, we have considered the following parameters without dimensions: $v = 1$, $l = 5$, $T = 15$. We have used the SLBM approach with:

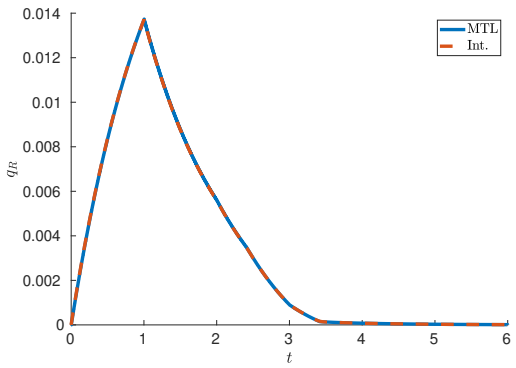

(a) reflectance q_r.

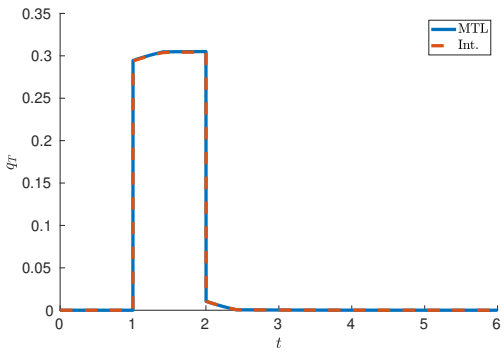

(b) transmittance q_t.

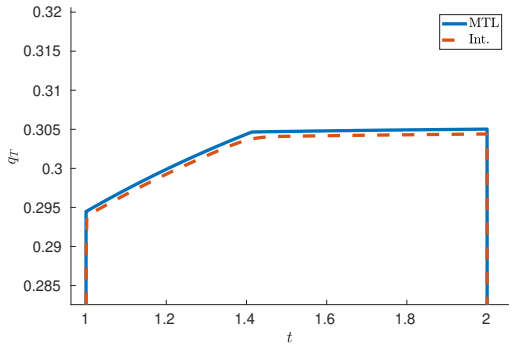

(c) zoom on (b).

Figure 12: Evolution of the reflectance q_r in (a) and transmittance q_t in (b) with a zoom on the upper part in (c), computed with the SLBM and space interpolation approaches with an albedo $\omega = 1.0$.

- a 2-dimensional lattice $\mathcal{L}_{\mathbf{x}}$, covering Ω with a constant step $\Delta x = 5/800$,
- a direction set $\mathcal{D}_9$ composed of 64 discrete directions,
- the 1-dimensional lattices associated to each subsets of $\mathcal{D}_9$.

The total energy we obtain is depicted by Figure 15 (a) at $t = 2.0$, (b) at $t = 4.0$ and (c) at $t = 6.0$. We also measure the backscattered flux q_a at point P_a whose coordinates are $\mathbf{x}_a = (-2.5, -0.5)$ defined as:

$$q_a(t) = \sum_{n=1}^{N_{\mathcal{S}}} \sum_{i=1}^{N^{I_n}} w_i^n |\mathbf{e}_1 \cdot \hat{\mathbf{k}}_i^{I_n}| a_i^n(t, \mathbf{x}_a). \tag{67}$$

The results we obtain for the case of a homogeneous medium (without the disc) and the heterogeneous one as well as those obtained in [27] are depicted by Figure 15 (d). In [27], the authors developed a radial basis function mesh-less method to numerically solve the spatial dependence. As one can observed, the two homogeneous solutions correspond well. For the heterogeneous case, we find the bump generated by the obstacle but less high compared to [27]. It is difficult to explain this difference, especially since neither solution can be considered an exact solution to the problem. However, we made sure to achieve convergence of our results as shown in Figure 16 where the evolutions of q_a at P_a for three increasingly large direction sets: $\mathcal{D}_2$, $\mathcal{D}_5$ and $\mathcal{D}_9$ are depicted for the homogeneous and heterogeneous medium cases (with $\Delta x = 5/800$).

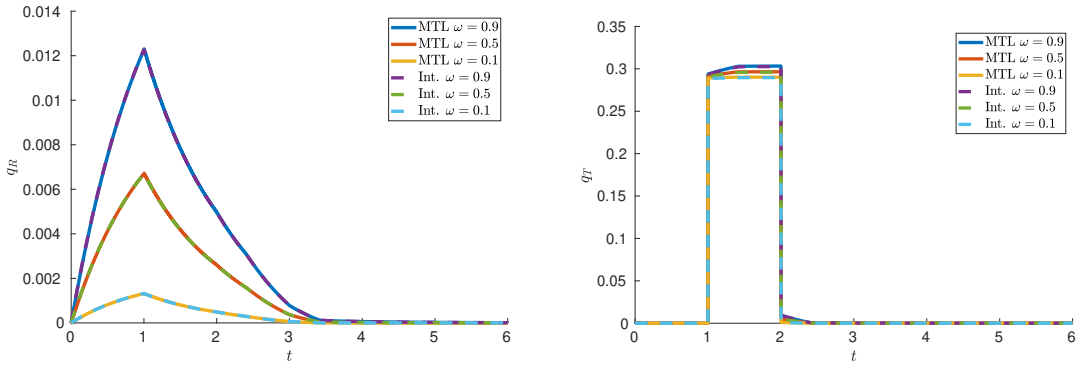

(a) reflectance q_r.

(b) transmittance q_t.

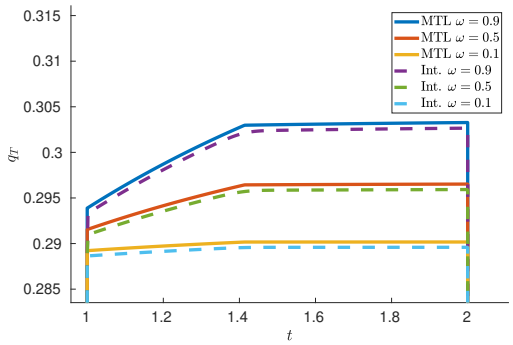

(c) zoom on (b).

Figure 13: Evolution of the reflectance q_r in (a) and transmittance q_t in (b) with a zoom on the upper part in (c), computed with the SLBM and interpolation approaches with different albedo values: $\omega = 0.9$, 0.5 and 0.1.

6. Conclusion

In this article, we proposed a new numerical approach, called the Staggered Lattice Boltzmann Method, which adapts some of the LBM features to the Radiative Transfer Equation solution. Its main highlights are:

- The definition of a SLBM formulation of the RTE, adapting some features of the LBM with different discretizations in time. The time incompatibilities being treated by a linear time interpolation.

- The construction of a particular discretization and quadrature for the unit sphere $\mathbb{S}^{d-1}$ following the DOM. This quadrature combine with the different time discretizations, allows to recover the particles *on-grid* streaming aspect of LBM.

- A traversal algorithm which allows to manage the incompatible time discretizations during the numerical resolution of the discrete RT problem. Each step of the algorithm starts by the determination of which direction the energy density is known and unknown at the considered time step. Then the algorithm imprints a second aspect of the LBM: the *collide-and-stream* paradigm, to solve the radiative transfer problem. The linear temporal interpolation step which precedes the collide one, shares the same local nature as this one. Indeed, it only involves data at the same space lattice node. It is this local nature which allows for massive parallelization.

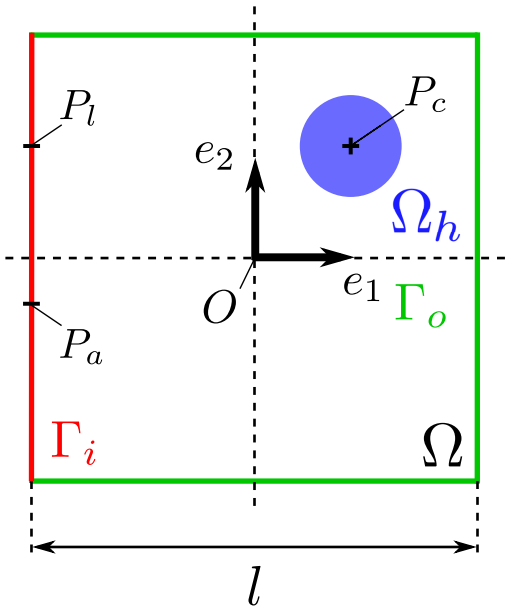

Figure 14: Geometry of the anisotropic and heterogeneous problem.

We consider that the Staggered Lattice Boltzmann Method approach, by all the common aspects it shares with the LBM, should reach the same efficiency level and then constitute a promising numerical method for the solution of the RTE.
We have successfully implemented our approach for the resolution of different two-dimensional problems and compare the solutions we obtained to the ones obtained with other approaches, found in literature. The comparison shows good agreement between the results.

Appendix A. Construction of a particular quadrature with prescribed nodes

We detail here how we proceeded to construct the quadratures we used to approximate the integral terms in the two-dimensional numerical tests ($d = 2$) presented in section 5, following the principle of the DOM. To do so, we assume that $N_{\mathcal{S}}$ direction sets, whose set of indexes is denoted $I \subset \mathbb{N}^\star$, have been chosen *a priori*. To conserve some symmetry in the quadrature, we chose to keep all the directions of each $\mathcal{S}_{I_n}$ ($n \in [\![1, N_{\mathcal{S}}]\!]$) set. We consider the set of chosen discrete directions constitute as a 1-dimensional lattice, denoted $\mathcal{L}_\theta$, of the 1-sphere and denote θ_i^n the polar angle associated to the direction $\hat{\mathbf{k}}_i^n$.
As mentioned in subsubsection 4.1, the quadrature we want to construct, for each discrete direction $\hat{\mathbf{k}}_i^n$, is given by equation (42), we recall here:

$$\int_{\mathbb{S}^1} \sigma(\hat{\mathbf{k}}_i^n \cdot \hat{\mathbf{k}}') a(t, \mathbf{x}, \hat{\mathbf{k}}') \, \mathrm{d}\hat{\mathbf{k}}' \approx \sum_{m=1}^{N_{\mathcal{S}}} \sum_{j=1}^{N^{I_m}} w_{ij}^{nm} a(t, \mathbf{x}, \hat{\mathbf{k}}_j^m), \tag{A.1}$$

with w_{ij}^{nm} the weight associated to the direction $\hat{\mathbf{k}}_i^n$. By decomposing the integral on each segment of $\mathcal{L}_\theta$ and approximating each term by the trapezoidal rule we obtain the following equation for the weights:

$$w_{ij}^{nm} = \frac{\theta^+ - \theta^-}{2} \sigma(\cos(\theta_i^n - \theta_j^m)) \tag{A.2}$$

where θ^- and θ^+ are the polar angles associated to the directions surrounding $\hat{\mathbf{k}}_j^m$ in $\mathcal{L}_\theta$ such that: $\theta^- < \theta_j^m < \theta^+$. We use exactly the same approach to approximate the energy density zeroth and first order moments (corresponding to the case $\sigma = 1$), giving:

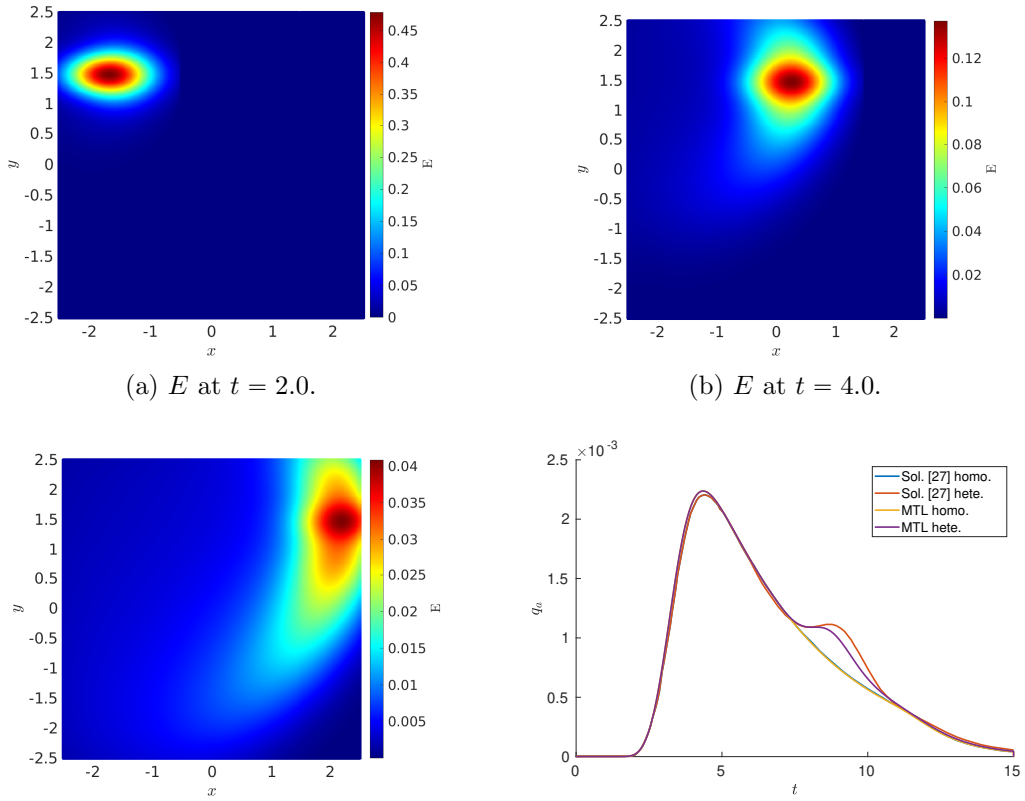

(a) E at $t = 2.0$. (b) E at $t = 4.0$.

(c) E at $t = 6.0$. (d) q_a at point P_a.

Figure 15: Evolution of the total energy E at $t = 2.0$ in (a), 4.0 in (b) and $t = 6.0$ in (c) for the heterogeneous medium case. Evolutions of the back-scattered flux q_a at point P_a for the homogeneous and heterogeneous medium cases one as well as those obtained in [27].

$$w_i^n = \frac{\theta^+ - \theta^-}{2}. \tag{A.3}$$

References

[1] S. Chandrasekhar, Radiative Transfer, Courier Corporation, 1960.

[2] M. F. Modest, S. Mazumder, Radiative heat transfer, Academic press, 2021.

[3] C. Villani, A review of mathematical topics in collisional kinetic theory, Handbook of mathematical fluid dynamics 1 (71-305) (2002) 3–8.

[4] L. Ryzhik, G. Papanicolaou, J. B. Keller, Transport equations for elastic and other waves in random media, Wave Motion 24 (4) (1996) 327–370.

[5] I. Baydoun, E. Savin, R. Cottereau, D. Clouteau, J. Guilleminot, Kinetic modeling of multiple scattering of elastic waves in heterogeneous anisotropic media, Wave Motion 51 (8) (2014) 1325–1348.

[6] A. Messaoudi, R. Cottereau, C. Gomez, Boundary effects in radiative transfer of acoustic waves in a randomly fluctuating half-space (2022).

[7] J. C. J. Paasschens, Solution of the time-dependent Boltzmann equation, Phys. Rev. E 56 (1997) 1135–1141.

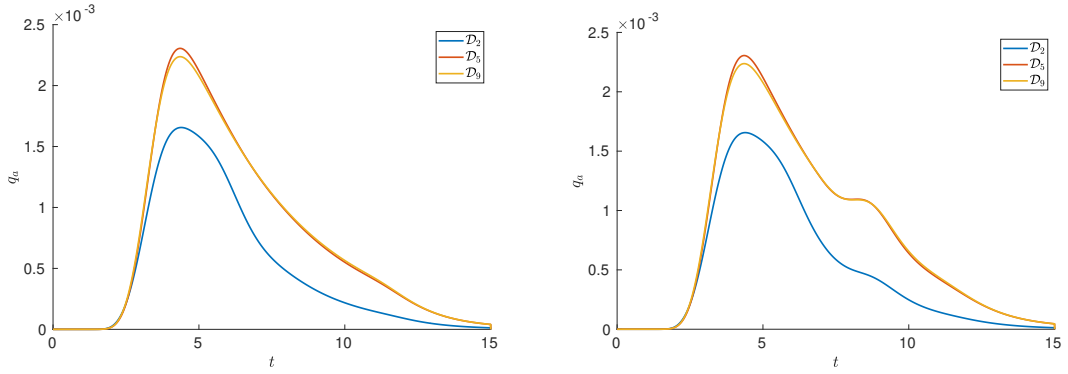

(a) homogeneous case. (b) heterogeneous case.

Figure 16: Evolutions of the back-scattered flux q_a at point P_a for three increasingly large direction sets: $\mathcal{D}_2$, $\mathcal{D}_5$ and $\mathcal{D}_9$ and for the homogeneous medium case in (a) and heterogeneous medium case in (b) (with $\Delta x = 5/800$).

[8] X. Liu, Y. Huang, C.-H. Wang, K. Zhu, A multiple-relaxation-time lattice Boltzmann model for radiative transfer equation, Journal of Computational Physics 429 (2021) 110007.

[9] H. C. Hottel, E. S. Cohen, Radiant heat exchange in a gas-filled enclosure: Allowance for nonuniformity of gas temperature, AIChE Journal 4 (1) (1958) 3–14.

[10] W. W. Yuen, E. E. Takara, The zonal method: a practical solution method for radiative transfer in nonisothermal inhomogeneous media, Annual Review of Heat Transfer 8 (1997) 153–215.

[11] C. Argento, D. Bouvard, A ray tracing method for evaluating the radiative heat transfer in porous media, International Journal of Heat and Mass Transfer 39 (15) (1996) 3175–3180.

[12] Y. Huang, G.-D. Shi, K.-Y. Zhu, Runge–kutta ray tracing technique for solving radiative heat transfer in a two-dimensional graded-index medium, Journal of Quantitative Spectroscopy and Radiative Transfer 176 (2016) 24–33.

[13] P. Rath, S. C. Mishra, P. Mahanta, U. K. Saha, K. Mitra, Discrete transfer method applied to transient radiative transfer problems in participating medium, Numerical Heat Transfer, Part A: Applications 44 (2) (2003) 183–197.

[14] N. A. Krishna, S. C. Mishra, Discrete transfer method applied to radiative transfer in a variable refractive index semitransparent medium, Journal of Quantitative Spectroscopy and Radiative Transfer 102 (3) (2006) 432–440.

[15] J. R. Howell, The Monte Carlo Method in Radiative Heat Transfer, Journal of Heat Transfer 120 (3) (1998) 547–560.

[16] H. Yong, S. Guo-Dong, Z. Ke-Yong, Backward and forward monte carlo method in polarized radiative transfer, The Astrophysical Journal 820 (1) (2016) 9.

[17] E. E. Lewis, W. F. Miller, Computational methods of neutron transport, John Wiley and Sons, Inc., New York, NY, 1984.

[18] J. C. Chai, H. S. Lee, S. V. Patankar, Finite volume method for radiation heat transfer, Journal of Thermophysics and Heat Transfer 8 (3) (1994) 419–425.

[19] J. Y. Murthy, S. R. Mathur, Finite volume method for radiative heat transfer using unstructured meshes, Journal of Thermophysics and Heat Transfer 12 (3) (1998) 313–321.

[20] L. Liu, L. Zhang, H. Tan, Finite element method for radiation heat transfer in multi-dimensional graded index medium, Journal of Quantitative Spectroscopy and Radiative Transfer 97 (3) (2006) 436–445.

[21] Y.-Y. Feng, C.-H. Wang, Discontinuous finite element method with a local numerical flux scheme for radiative transfer with strong inhomogeneity, International Journal of Heat and Mass Transfer 126 (2018) 783–795.

[22] R. Koch, R. Becker, Evaluation of quadrature schemes for the discrete ordinates method, Journal of Quantitative Spectroscopy and Radiative Transfer 84 (4) (2004) 423–435, eurotherm Seminar 73 - Computational Thermal Radiation in Participating Media.

[23] S. Rukolaine, V. Yuferev, Discrete ordinates quadrature schemes based on the angular interpolation of radiation intensity, Journal of Quantitative Spectroscopy and Radiative Transfer 69 (3) (2001) 257–275.

[24] P. J. Coelho, Advances in the discrete ordinates and finite volume methods for the solution of radiative heat transfer problems in participating media, Journal of Quantitative Spectroscopy and Radiative Transfer 145 (2014) 121–146.

[25] J. Moreno, C. Casado, J. Marugán, Improved discrete ordinate method for accurate simulation radiation transport using solar and led light sources, Chemical Engineering Science 205 (2019) 151–164.

[26] J. Zhao, J. Tan, L. Liu, A second order radiative transfer equation and its solution by meshless method with application to strongly inhomogeneous media, Journal of Computational Physics 232 (1) (2013) 431–455.

[27] M. Kindelan, F. Bernal, P. González-Rodríguez, M. Moscoso, Application of the rbf meshless method to the solution of the radiative transport equation, Journal of Computational Physics 229 (5) (2010) 1897–1908.

[28] A. C. Hughes, A. G. Buchan, An adaptive reduced order model for the angular discretization of the Boltzmann transport equation using independent basis sets over a partitioning of the space-angle domain, International Journal for Numerical Methods in Engineering 123 (16) (2022) 3781–3799.

[29] Y. Feng, P. Sagaut, W.-Q. Tao, A compressible lattice Boltzmann finite volume model for high subsonic and transonic flows on regular lattices, Computers and Fluids 131 (2016) 45–55.

[30] G. Farag, S. Zhao, T. Coratger, P. Boivin, G. Chiavassa, P. Sagaut, A pressure-based regularized lattice-Boltzmann method for the simulation of compressible flows, Physics of Fluids 32 (6) (2020) 66106.

[31] F. Dubois, Equivalent partial differential equations of a lattice Boltzmann scheme, Computers and Mathematics with Applications 55 (7) (2008) 1441–1449.

[32] G. Farag, S. Zhao, G. Chiavassa, P. Boivin, Consistency study of lattice-boltzmann schemes macroscopic limit, Physics of Fluids 33 (3) (2021) 031701.

[33] T. Bellotti, Rigorous derivation of the macroscopic equations for the lattice Boltzmann method via the corresponding finite difference scheme, working paper or preprint (May 2022).

[34] T. Bellotti, B. Graille, M. Massot, Finite difference formulation of any lattice Boltzmann scheme, working paper or preprint (May 2022).

[35] P. Asinari, S. C. Mishra, R. Borchiellini, A lattice Boltzmann formulation for the analysis of radiative heat transfer problems in a participating medium, Numerical Heat Transfer, Part B: Fundamentals 57 (2) (2010) 126–146.

[36] S. C. Mishra, H. Poonia, R. R. Vernekar, A. K. Das, Lattice Boltzmann method applied to radiative transport analysis in a planar participating medium, Heat Transfer Engineering 35 (14-15) (2014) 1267–1278.

[37] C. McHardy, T. Horneber, C. Rauh, New lattice Boltzmann method for the simulation of three-dimensional radiation transfer in turbid media, Opt. Express 24 (15) (2016) 16999–17017.

[38] Y. Wang, Y. Ma, M. Xie, High-order lattice Boltzmann method for multi-group neutron diffusion solution, Progress in Nuclear Energy 110 (2019) 341–353.

[39] A. Mink, C. McHardy, L. Bressel, C. Rauh, M. J. Krause, Radiative transfer lattice Boltzmann methods: 3d models and their performance in different regimes of radiative transfer, Journal of Quantitative Spectroscopy and Radiative Transfer 243 (2020) 106810.

[40] A. Mink, G. Thäter, H. Nirschl, M. J. Krause, A 3d lattice Boltzmann method for light simulation in participating media, Journal of Computational Science 17 (2016) 431–437.

[41] H.-L. Yi, F.-J. Yao, H.-P. Tan, Lattice Boltzmann model for a steady radiative transfer equation, Phys. Rev. E 94 (2016) 023312.

[42] Y. Wang, L. Yan, Y. Ma, Lattice Boltzmann solution of the transient Boltzmann transport equation in radiative and neutron transport, Phys. Rev. E 95 (2017) 063313.

[43] M. Zhang, W. Zhao, P. Lin, Lattice Boltzmann method for general convection-diffusion equations: Mrt model and boundary schemes, Journal of Computational Physics 389 (2019) 147–163.

[44] B. Shi, Z. Guo, Lattice Boltzmann model for nonlinear convection-diffusion equations, Phys. Rev. E 79 (2009) 016701.

[45] L. Weih, A. Gabbana, D. Simeoni, L. Rezzolla, S. Succi, R. Tripiccione, Beyond moments: relativistic lattice Boltzmann methods for radiative transport in computational astrophysics, Monthly Notices of the Royal Astronomical Society 498 (3) (2020) 3374–3394.

[46] B. J. Cantwell, Fundamentals of compressible flow (January 2022).

[47] P. L. Bhatnagar, E. P. Gross, M. Krook, A model for collision processes in gases. i. small amplitude processes in charged and neutral one-component systems, Phys. Rev. 94 (1954) 511–525.

[48] S. Succi, The lattice Boltzmann equation: for fluid dynamics and beyond, Oxford university press, 2001.

[49] T. Krüger, H. Kusumaatmaja, A. Kuzmin, O. Shardt, G. Silva, E. M. Viggen, The lattice Boltzmann method, Springer International Publishing 10 (978-3) (2017) 4–15.

[50] J. C. M. M.A., V. Illustrations of the dynamical theory of gases.—Part I. On the motions and collisions of perfectly elastic spheres, The London, Edinburgh, and Dublin Philosophical Magazine and Journal of Science 19 (124) (1860) 19–32.

[51] C. Bardos, E. Bernard, F. Golse, R. Sentis, The diffusion approximation for the linear Boltzmann equation with vanishing scattering coefficient, Communications in Mathematical Sciences 13 (3) (2015) 641–671.

[52] R. Koch, W. Krebs, S. Wittig, R. Viskanta, Discrete ordinates quadrature schemes for multidimensional radiative transfer, Journal of Quantitative Spectroscopy and Radiative Transfer 53 (4) (1995) 353–372.

[53] R. Koch, R. Becker, Evaluation of quadrature schemes for the discrete ordinates method, Journal of Quantitative Spectroscopy and Radiative Transfer 84 (4) (2004) 423–435, eurotherm Seminar 73 - Computational Thermal Radiation in Participating Media.

[54] K. Atkinson, W. Han, Spherical harmonics and approximations on the unit sphere: an introduction, Vol. 2044, Springer Science & Business Media, 2012.

[55] L. C. Henyey, J. L. Greenstein, Diffuse radiation in the galaxy, The Astrophysical Journal 93 (1940) 70–83.